/CDF/PHYS/BOTTOM/CDFR/6288
Version 4.0
April 8, 2004

Measurement of the Run-II Inclusive J/ψ Cross-section

Tomohiro Yamashita[1], Slawomir Tkaczyk[2], Ting Miao[2], Dmitri Litvintsev[2], Jonathan Lewis[2] Thomas LeCompte[3], James Kraus[4], Yuri Gotra[5], Mary Bishai[2]

[1] *Okayama University*
[2] *Fermi National Accelerator Laboratory*
[3] *Argonne National Lab* [4] *University of Illinois*
[5] *University of Pittsburgh*

Abstract

Using a 39.7 pb^{-1} Run-II data sample collected from February to October 2002, a new measurement of the inclusive J/ψ cross-section has been performed. The J/ψ events were collected using the CMU-CMU di-muon triggers, and the raw yields were corrected by the geometric and kinematic acceptance, trigger efficiency and reconstruction efficiency. A p_T dependent differential cross section has been calculated for events with rapidity $|y| < 0.6$. The total integrated cross section for inclusive J/ψ production in $p\bar{p}$ interactions at C.O.M. energy, $\sqrt{s} = 1960$ GeV/c^2, is measured to be:

$$\sigma(p\overline{p} \to J/\psi X, \mid y(J/\psi) \mid < 0.6) \cdot Br(J/\psi \to \mu\mu) = 240 \pm 1(stat) \pm 21(syst) \text{ nb}$$

.

Contents

1 Introduction

The production mechanisms of J/ψ in $p\bar{p}$ collisions are not well understood. Production cross sections from the assumed two major sources, $b \rightarrow J/\psi X$ and direct prompt decays, were measured to be higher than the initial theoretical predictions [1]. Recent theoretical advances in the extraction of the non-perturbative fragmentation functions of the B mesons from LEP data in a way that is consistent with the NLO QCD calculations of the b hadroproduction cross-sections have improved agreement between theoretical predictions and CDF Run I $b \rightarrow J/\psi X$ cross-section mesurements to better than 50% [2] [3].

Non-relativistic quarkonia bound states are best described by Non-Relativistic QCD (NRQCD) theoretical models which are used to predict the hadroproduction cross-sections [4] [5]. At large transverse momenta, fragmentation type production dominates and color-octet matrix elements dominate the color-singlet matrix element contribution [6]. The results agree well with data at the Tevatron for $p_T(J/\psi) > 5$ GeV/c, as shown in Figure 1.

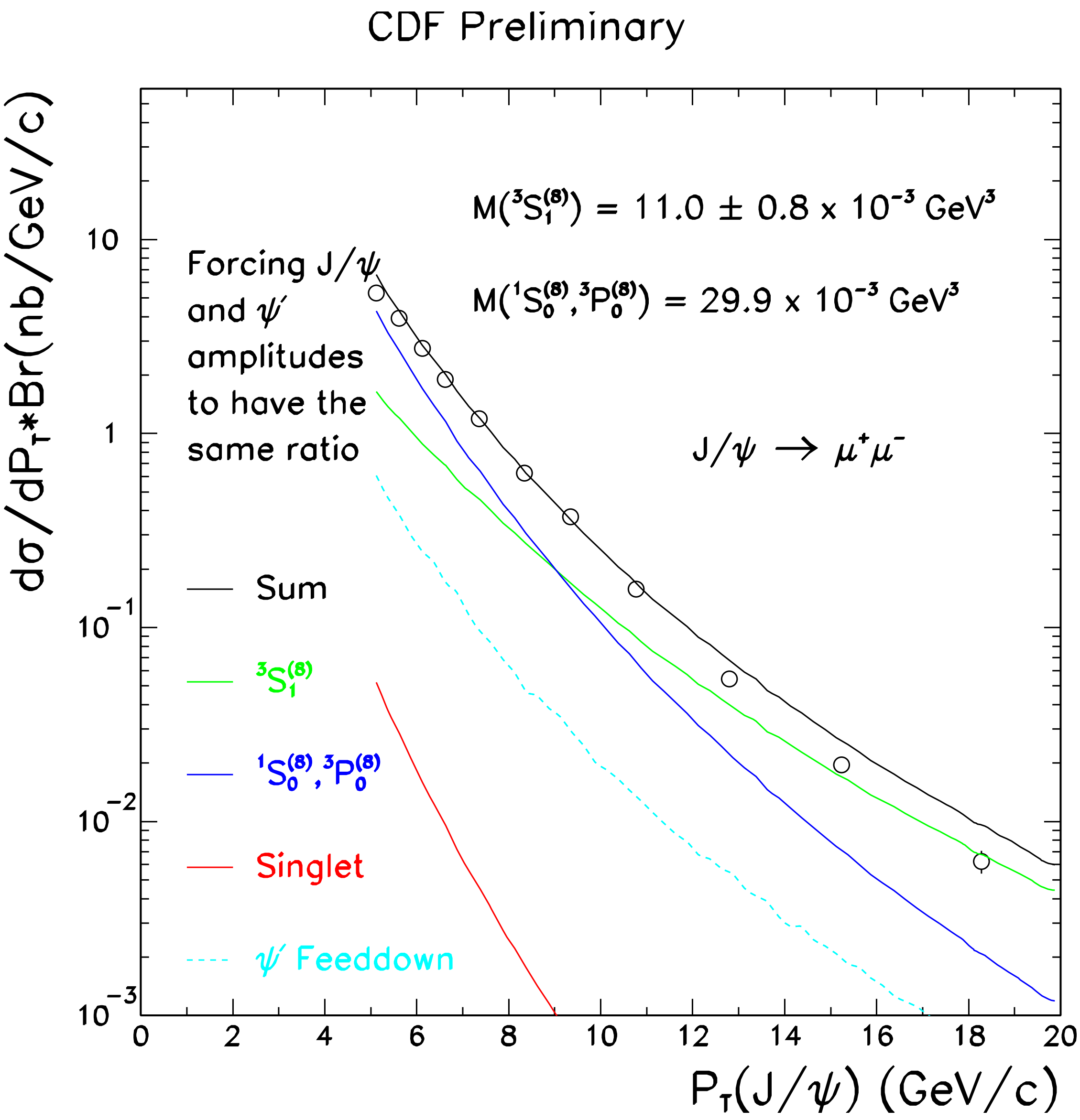

Figure 1: Direct CDF Run I J/ψ production data and theoretical predictions

At low transverse momenta, soft gluon effects and non-fragmentation effects from other octet matrix elements that are difficult to calculate theoretically become important and cause theory predictions and data to diverge. The Run I measurements of the Upsilon(nS) cross-sections at small transverse momenta [7] indicate that data and theory diverge at transverse momenta < 6 GeV/c.

The Run-II CDF detector has an improved dimuon trigger with a lower p_T threshold of > 1.4 GeV/c. This has extended the low transverse momentum range of triggered $J/\psi \to \mu\mu$ events down to $p_T(\mu\mu) \geq 0$ GeV/c. A new measurement of the total inclusive J/ψ cross-section using Run-II data has been carried out. This note summarizes the status of the Run-II measurement of the inclusive J/ψ cross-section.

2 Data sample and event selection

The $J/\psi \to \mu^+\mu^-$ sample used for this analysis was collected using the CMU-CMU dimuon triggers. The efficiency and performance of the L1 and L3 dimuon triggers as measured w.r.t to offline muon and COT reconstruction are described in detail in [8] and [9]. The data sample used comprises runs in the range 138425-152625 (excluding 152620, 152623) that correspond to the stable running period of February to October 2002. The 2-miss Level 1 XFT trigger algorithim and version 4.3.0 of the L3 trigger reconstruction software was used to collect the data. For the dimuon triggers, the level 2 performs an auto-accept of level 1. Two level 3 trigger paths are used for this cross-section measurment JPSI_CMUCMU1.5, and JPSI_CMUCMU1.5_ALLPHI. The JPSI_CMUCMU1.5_ALLPHI L3 path was introduced after run 150010. There is no dimuon opening angle requirement in JPSI_CMUCMU1.5_ALLPHI, whereas there is a requirement that the dimuon opening angle in the $r - phi$ plane is $> 128.9^0$ in JPSI_CMUCMU1.5. Therefore, we use the run range 150010 - 152625 for the measurement of the cross-section in the J/ψ transverse momentum range of 0 - 2 GeV/c, and the full run range for measurements of the cross-section from 2 to 20 GeV/c.

2.1 Good run selection

Runs marked as "Good" by data taking shift crews online were further analyzed offline to exclude those with COT, muon or trigger hardware problems [1]. The total luminosity and number of runs accepted after each online and offline validation requirement is summarized in Table 1

The run by run J/ψ yield, invariant mass mean, and width is determined from a single Gaussian fit to the di-muon invariant mass distribution with a first order polynomial for the background. The number of J/ψs reconstructed is normalized by the luminosity. Yields, reconstructed mass and width of J/ψ from the 4.8.4a production data for runs that passed the COT and CMU offline validation requirements were carefully examined [13]. The CMU-CMU J/ψ rate measured in runs 138425 to 152625 for all runs with luminosities $> 10\text{nb}^{-1}$ is shown in Figure 2; runs that failed the online and offline good run selection are marked as open circles. To identify

[1] Silicon detector tracking information is not used in this measurement.

Run quality requirement	Number of runs	Luminosity (nb^{-1})
None	14106	59,505
GoodRun(RunControl)*	766	54,335
+CLC_STATUS	664	51,458 **
+L1,2,3_STATUS	612	48,887
+OFFLINE_STATUS [10]	572	47,671
+COT_OFFLINE [11]	467	39,854
+CMU_OFFLINE [12]	458	39,096
Good run sections on CAF	457	39,000

Table 1: Number of runs and integrated luminosities after various online and offline database good run bit requirements. For runs from 138425-152625. * GoodRun requirements correspond to the following data file catalog database bits: RUNCONTROL_STATUS, SHIFTCREW_STATUS. ** After these requirements there are no runs with integrated live luminosities of < 10 nb^{-1}

remaining runs which may have additional hardware or trigger problems that have been undetected by the standard COT/CMU offline validation criteria, good runs with J/ψ yields different by 4σ from the run averaged yield, where σ is the standard deviation of the yields in a given run range, are marked as red triangles. Two runs out of 457 are found to have yields different by 4σ from the average where the expected number is 0.03 (Chauvenet's criterion [14]). The run numbers are 143938 (14.314 nb^{-1}), and 152579 (258.286 nb^{-1}). Preliminary investigations of online operational conditions during both of these runs revealed no obvious hardware or trigger malfunctions. Both runs are included in the base-line cross-section measurement. The measurement is repeated without the suspicious runs included and a systematic uncertainty assigned.

The final selected collection of high quality events are from runs 138819 to 152625 and corresponds to a total default luminosity of 39.0 ± 2.3 pb^{-1}. The luminosity is obtained from the CDF offline database file catalog (DFC) for each run section from which the primary dataset was obtained [15]. A correction factor of +1.9% is applied to the luminosity values obtained from the DFC at this time [17] such that the luminostity to be used for the cross-section measurement is 39.7 ± 2.3 pb^{-1} for the whole sample and 14.83 ± 0.87 pb^{-1} for the ALLPHI portion of the data sample. The 5.9% uncertainty on the luminosity is the combined systematic uncertainty from the CLC acceptance [16] (4.4%) [2] assigned to the luminosity delivered to disk and the uncertainty on the inelastic $p\bar{p}$ crossection [17] (4.0%).

Table 2 summarizes the data sample and final luminosities used in this measurement.

[2]Blessed

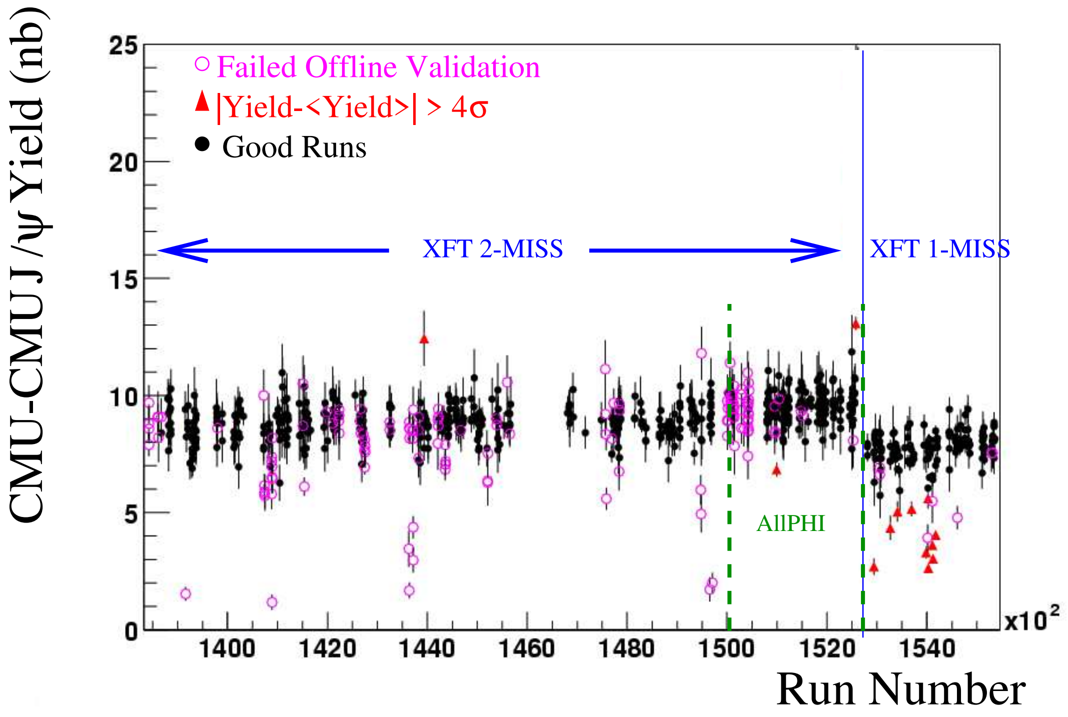

Figure 2: J/ψ signal rate from the total and CMU-CMU trigger as a function of run number for data collected Feb 2002 to Dec 2002. Only the XFT 2-miss run range is used for the Run II J/ψ cross-section measurement.

2.2 J/ψ event selection

$J/\psi \rightarrow \mu^+\mu^-$ decays were reconstructed in the data sample processed with CDF offline software version 4.8.4. Both muons are required to be confirmed CMU or CMUP muons with $\chi^2(\Delta r\phi)_{CMU} < 9$ [18] in addition to the default CMU muon reconstruction selection criteria in the muon reconstruction package [3]. Both muons

[3] The default matching criteria used in CMU muon reconstruction is $\Delta(r\phi)_{CMU} < 30cm$. The track is required to point to the same side (E/W) of the detector that the stub is in, unless the muon is near the E/W boundary, in which case a 20 cm match is required.

Run range	J/ψ L3 Trigger used	Good run luminosity (pb^{-1})	J/ψ p_T range
138425 - 150009	JPSI_CMUCMU1.5	39.7 ± 2.3	2-20 GeV/c
150010 - 152625	JPSI_CMUCMU1.5_ALLPHI	14.83 ± 0.87	0 -2 GeV/c

Table 2: Data sample used and corresponding luminosity.

were required to be CMU muons and have $p_T > 1.5$ GeV/c as measured in the COT. The invariant mass was calculated from the four-momenta of the two muons using COT tracks, and no vertex fitting was applied. Both reconstructed muons are required to match the triggered di-muon L1 stub pair and the corresponding XFT tracks. The details of the matching algorithim used to match L1 and L3 triggered muons to the offline reconstructed muons is described in [8] and [9]. Furthermore, each event is required to be tagged as a Level 3 JPSI_CMUCMU1.5 or JPSI_CMUCMU1.5_ALLPHI. A hardware problem with the L1 dimuon matchbox logic prior to run 150143 caused the trigger to exclude J/ψ events where both muon stubs fall into the *phi* range of $240 - 270^0$ [8]. This hardware problem was fixed for runs > 150143. For uniformity, J/ψ events where both muons fall in the matchbox 8 region are rejected in the cross-section calculation for the whole data sample under consideration. As discussed in [8], the L1 tracking trigger efficiency is lower and not well modeled when tracks pass close to the center of the COT wire plane in either of the 4 axial superlayers. J/ψ events where either one of the tracks passed within 1.5 cm of the center of the wire planes are rejected and will be corrected for in the acceptance calculation. The muon reconstruction efficiency is measured in each of the 42 CMU detector wedges. The efficiency in wedge 17West is found to be lower due to a known hardware problem caused by a short on one of the HV lines [22]. J/ψ events where either μ stub was reconstructed in 17W are excluded from the cross-section calculation and taken into account in the acceptance calculation.

The selection criteria applied at different stages of event selection are summarized as follows:

- *L1 selection criteria:*
  - $p_T(\mu)_{XFT} > 1.5$ GeV/c
  - Muon stubs matched triggered stubs
  - Di-muon candidate stubs are seperated by 2 CMU 2.4^0 towers.
  - Muon tracks matched to XFT tracks and XTRP projections
  - Exclude tracks which pass within 1.5 cm of the center of the COT wire planes in any of the 4 axial layers.
  - Exclude events where both muon stubs fall in the range $240-270^0$ (matchbox 8 problem [8]).
- *L2 selection criteria:* None
- *L3 selection criteria:*

- CMU muons
- $p_T(\mu)_{COT} > 1.5$ GeV/c
- Opposite sign muons
- $|z_0(\mu_1) - z_0(\mu_2)| < 5$ cm
- $2.7 < M(\mu\mu) < 4.0$ GeV/c^2
- $\Delta\phi(\mu\mu) < 130^0$ when $p_T(J/[y]) > 2.0$ GeV/c
- stub-track match: $\Delta(r\phi)_{CMU} < 30cm$

- *Additional offline selection:*
  - Explicitly require CMU-only or CMUP muons
  - $\chi^2(\Delta r\phi)_{CMU} < 9$
  - $\mid y(J/\psi) \mid < 0.6$
  - COT hits: axial$\geq$ 20, stereo$\geq$ 16.
  - $|z0(\mu)| < 90$ cm
  - Exclude muons in CMU wedge 17W

To correct the muon momentum for energy loss in the silicon detector, each muon COT track was refit using version 4.9.1 of the SiTrackFitter module and the corresponding silicon material description in GEANT [4]. A B-field correction factor of 1.0013 [19] was also applied to the refit momenta of the muons. Figure 3 shows the $\mu\mu$ invariant mass distribution for all the selected events in the range $2.7 < M(\mu\mu) < 3.5$ GeV/c^2. From a fit to a double Gaussian and a 2$^{\text{nd}}$ order polynomial background, the total number of J/ψ reconstructed for this study is $299,800 \pm 800$ with an invariant mass of 3.09391 ± 0.00008 GeV/c^2 and an average width of 0.020 ± 0.001 GeV/c^2.

The reconstructed J/ψ invariant mass is 3 MeV/c^2 lower than the current world average of 3.09688 ± 0.00004 GeV/c^2 [20]. This has been attributed to an underestimation of the energy loss in the silicon detector due to an incomplete accounting of the material in the SVXII detector [19]. A systematic error of +0.1% on the momentum scale in each J/ψ bin will be added to account for the underestimation of the energy loss in the tracking chambers.

3 J/ψ Yield

To estimate the correct yield in each p_T bin, the J/ψ invariant mass signal distribution including the radiative tail is fitted using the COT shapes obtained from the tuned

[4]No silicon hits were added during the refit

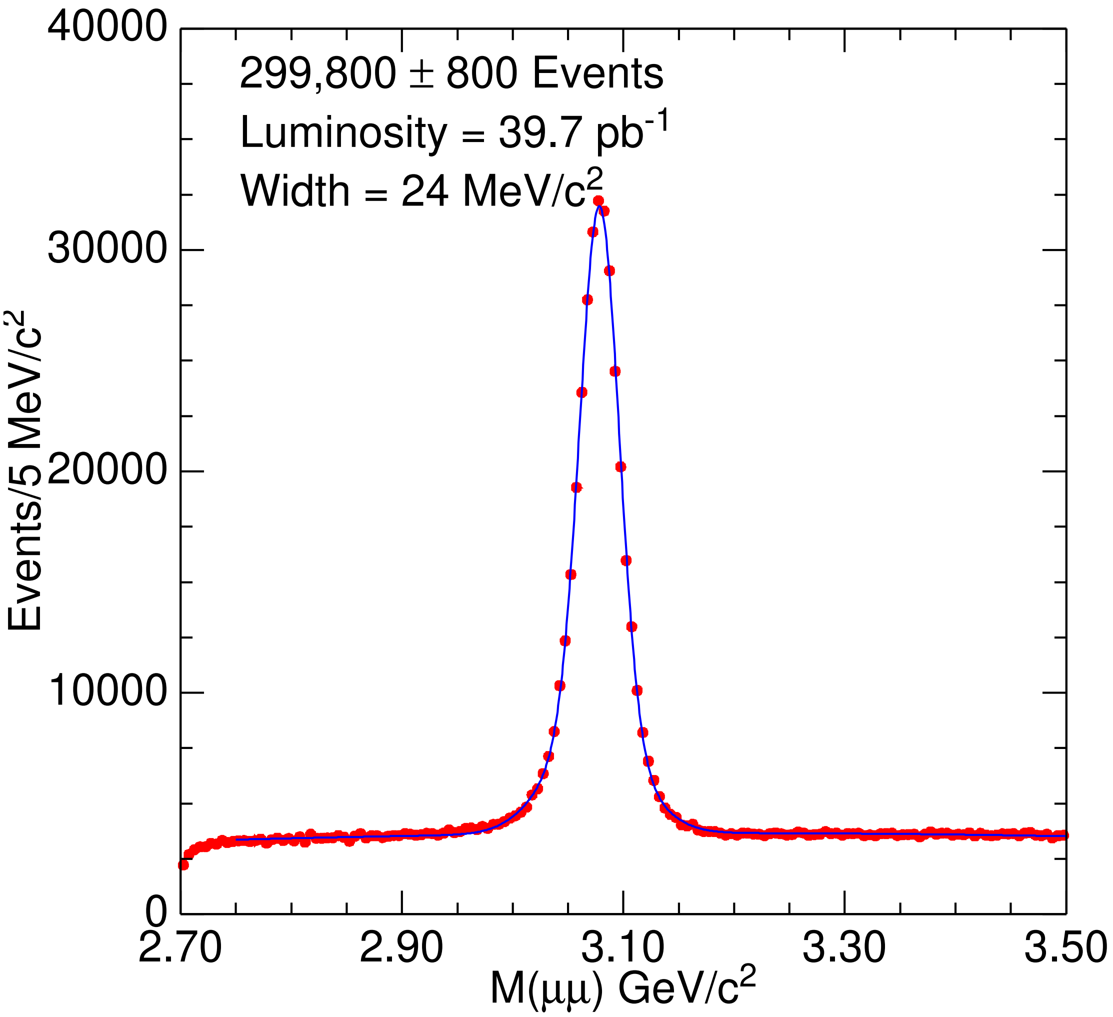

Figure 3: Invariant mass distribution of reconstructed $J/\psi \to \mu\mu$ candidates.

hit level simulation [24]. J/ψ events are decayed using the ψ radiative decay model in the QQ decay package. Firstly, the COT hit multiplicity per track is tuned to match the data as closely as possible as shown in Figure 4. The hit level simulation is too simplistic to obtain a perfect match with data and there is no differentiation between the hit distributions in the different superlayers. Secondly, the COT hit resolution is then tuned till the best $\chi^2/D.O.F.$ is obtained from a binned likelihood fit to the data using the MC invariant mass shape for the signal and a Chebyshev polynomial shape for the background. The order of the polynomial used varies with the background shape in each J/ψ p_T range. A 3^{rd} order polynomial is used in the momentum range 0-250 MeV/c, a 2^{nd} order polynomial is used to model the background shape in the

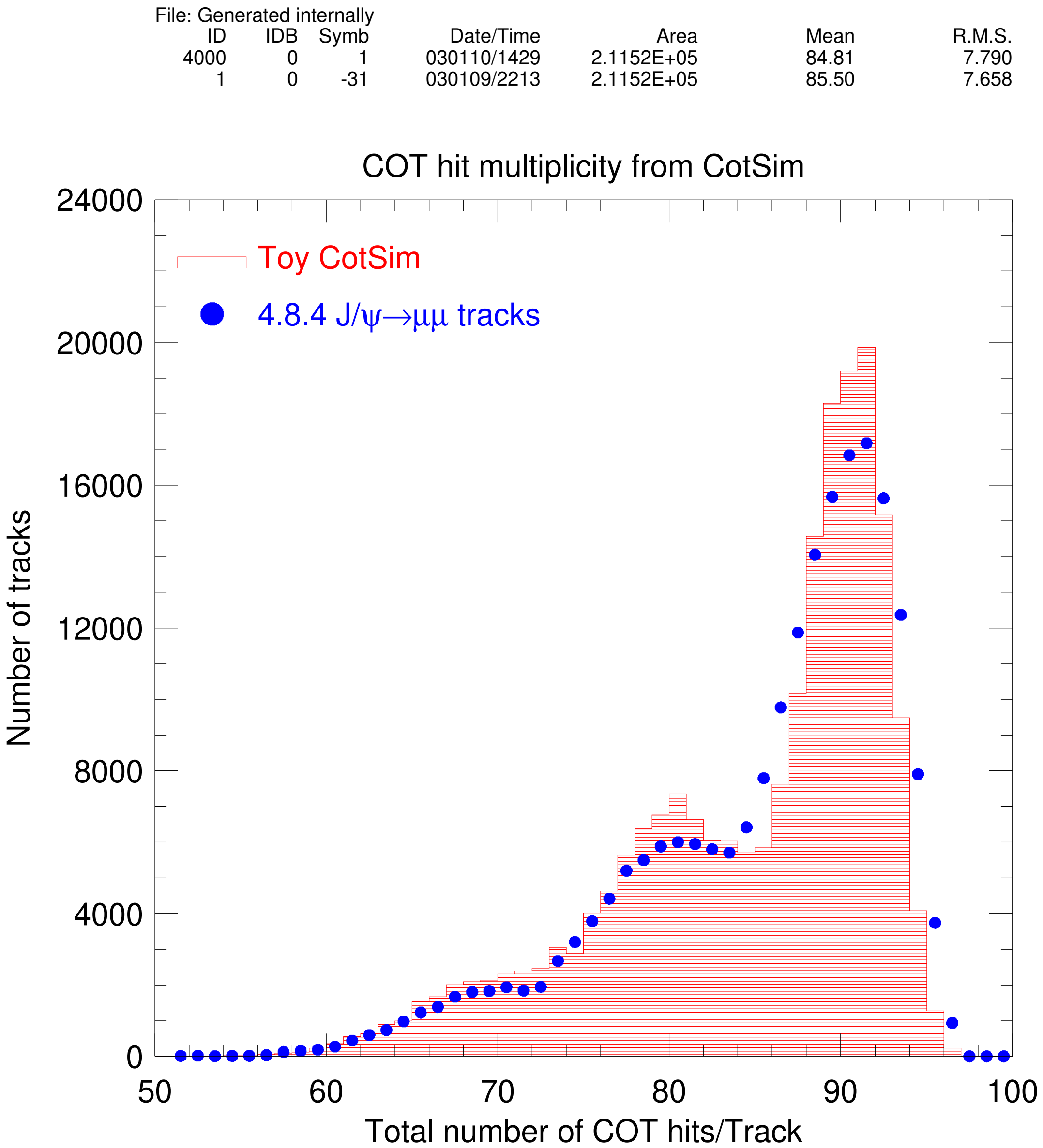

Figure 4: COT hit multiplicity distributions on J/ψ muon tracks obtained using the simple hit level simulation (shaded histogram) as compared to data (points with error bars)

range 0.25-2.25 GeV/c and a 1^{st} order polynomial for J/ψ with transverse momenta $>$ 2.25 GeV/c. Lastly, energy loss and multiple scattering in upstream material are modeled using the Silimap material description v4.9.1. The SVXII material is scaled until the peaks of the J/ψ raw COT invariant mass distribution ins different p_T bins in data and from the simulation match up. The best COT resolution was found to be 210μm and a 10% increase in SVXII material was required to best fit the data. The tuned COT resolution is larger than that measured in data (180μm) because the MC overestimates the number of hits/track.

The fits to the raw COT invariant mass distributions in three sample bins are shown in Figure 5.

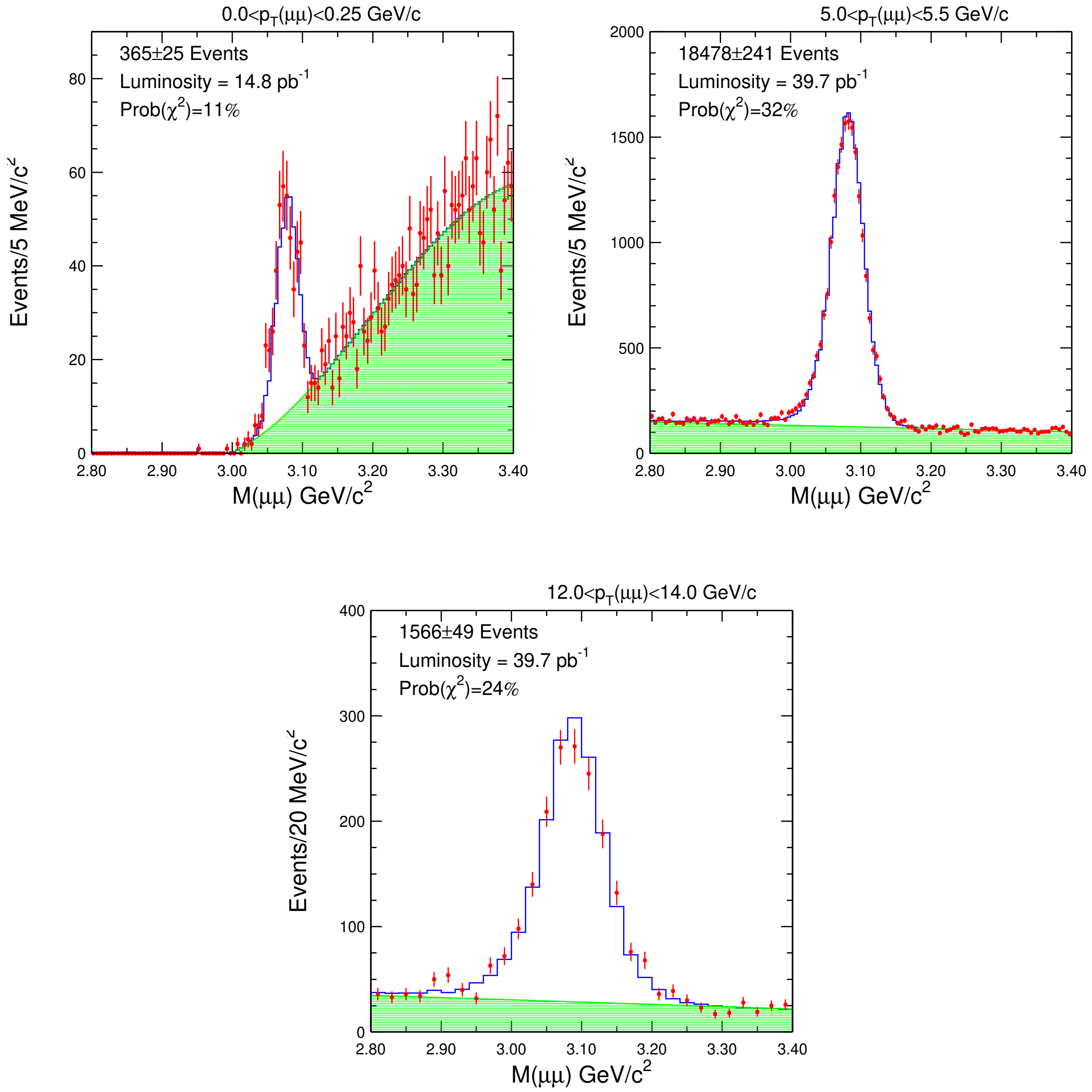

Figure 5: Invariant mass distributions of reconstructed $J/\psi \rightarrow \mu\mu$ events. The points with error bars are data. The solid line is the fit to the signal shape from the simulation and an n$^t h$ order Chebyshev polynomial for the background. The shaded histogram is the fitted background shape.

The yields and the statistical errors obtained from the fits are indicated in the first column of Table 3.

3.1 Systematic uncertainties and Goodness-of-Fit

The fit prob(χ^2) in each $p_T(J/\psi)$ bin is listed in Table 3 and indicates that the invariant mass fit in most bins is a good fit. A qualitative estimate of the goodness-of-fit is be obtained by defining a quality factor R such that

$$R = \Sigma_i(N_i - N_f) \tag{1}$$

where N_i is the number of data events in the i^{th} invariant mass bin and N_f is the fit prediction. For perfect fits, this factor should be consistent with 0. The summation is performed over bins in the invariant mass signal region from 3.02 to 3.15 where the J/ψ signal dominates the background. Deviations from 0 indicate a discrepency in the yield that is a good estimate of the systematic error on the yield in each p_T bin. Table 3 summarizes the fraction of the data that is not accounted for in the mass fit where it is assumed that the difference in the fit and data results could all be attributed to the J/ψ signal yield. The largest discrepencies are in the bins 0 to 2 GeV/c where the background function is rapidly changing under the signal peak. The fractional disagreement between data and the fit function for bins $>$ 2 GeV/c is less than 1%. The ratio of $R/yield$ is taken as the fractional systematic uncertainty on the yield.

4 Reconstruction efficiencies

In CDF Run II, a muon is reconstructed from a track matched to a stub in the muon chambers. The triggers from which the J/ψ is obtained only use COT tracks matched to CMU stubs (or CMX). The total reconstruction efficiency is divided into several parts that are measured seperately with care to ensure compatibility. The total reconstruction efficiency, independant of the detector acceptance is given by:

$$\epsilon_{reco}^{all} = \frac{\text{L1\&L3\&Offline}}{\text{L3\&Offline}} \times \frac{\text{L3\&Offline}}{\text{Offline}} \times \text{CotTrack}_{reco}^{offline} \times \text{CdfMuon}_{reco}^{offline} \tag{2}$$

where L3&Offline indicates a muon reconstruced in L3 that has also been matched to an offline reconstructed muon.

4.1 Level 1 trigger efficiency

The Run II L1 single CMU muon trigger efficiency measured versus L3 muons that are matched to an offline reconstructed muon was measured in [8]. This efficiency is applicable to L1 muons that triggered using the 2-miss XFT algorithim and is found to be a function of only $p_T(\mu)$ when tracks passing within 1.5 cm of the center of the COT wire planes in any of the axial layers are excluded. The single muon Level 1

P_t range GeV/c	Yield MC shape	Prob(χ^2)	$R = \Sigma_i(N_i - N_f)$ 3.02-3.15 GeV/c^2(%)
$0.0 - 0.25$	365 ± 25	0.108205	8.9
$0.25 - 0.5$	605 ± 30	0.418785	5.9
$0.5 - 0.75$	962 ± 38	0.172044	4.4
$0.75 - 1.0$	1592 ± 49	0.0340090	4.4
$1.0 - 1.25$	2500 ± 62	0.707163	1.6
$1.25 - 1.5$	3549 ± 74	0.265929	1.4
$1.5 - 1.75$	4517 ± 84	0.034378	1.9
$1.75 - 2.0$	5442 ± 93	0.105880	1.3
$2.0 - 2.25$	16059 ± 167	8.327424E-06	0.9
$2.25 - 2.5$	18534 ± 252	8.152634E-05	0.6
$2.5 - 2.75$	18437 ± 253	0.027786	0.4
$2.75 - 3.0$	18858 ± 259	0.236414	0.5
$3.0 - 3.25$	18101 ± 253	0.027021	0.3
$3.25 - 3.5$	17597 ± 250	0.272719	0.3
$3.5 - 3.75$	16400 ± 241	0.148081	0.1
$3.75 - 4.0$	14863 ± 226	0.063650	0.06
$4.0 - 4.25$	14056 ± 218	0.679069	-0.3
$4.25 - 4.5$	12719 ± 212	0.041509	-0.3
$4.5 - 4.75$	12136 ± 201	0.775579	-0.3
$4.75 - 5.0$	10772 ± 188	0.933651	-0.4
$5.0 - 5.5$	18478 ± 241	0.316311	-0.4
$5.5 - 6.0$	14616 ± 210	0.212992	-0.7
$6.0 - 6.5$	11388 ± 180	0.473387	-0.7
$6.5 - 7.0$	8687 ± 154	0.515111	-1.3
$7.0 - 8.0$	12409 ± 139	0.989518	-0.3
$8.0 - 9.0$	6939 ± 107	0.095595	-0.8
$9.0 - 10.0$	3973 ± 78	0.926075	-0.7
$10.0 - 12.0$	3806 ± 74	0.561407	-0.6
$12.0 - 14.0$	1566 ± 49	0.239436	-0.3
$14.0 - 17.0$	935 ± 40	0.416051	0.9
$17 - 20.0$	350 ± 25	0.319768	2.3

Table 3: J/ψ invariant yield in different J/ψ transverse momentum bins. Goodness-of-fit and systematic uncertainties are also listed.

trigger efficiency measurement is shown in Figure 6. The central value of the data distribution is fit to the following function:

$$\epsilon^{\mu}_{L1}(p^{\mu}_{T}) = (0.9774 \pm 0.0020) \times freq\left(\frac{(1.10 \pm 0.11) - 1/p_T}{(0.276 \pm 0.060)}\right) \tag{3}$$

where $freq$ is the normal frequency function:

$$freq(x) = \frac{1}{\sqrt{2\pi}} \int_{-\infty}^{x} e^{-\frac{1}{2}t^2} dt$$

:

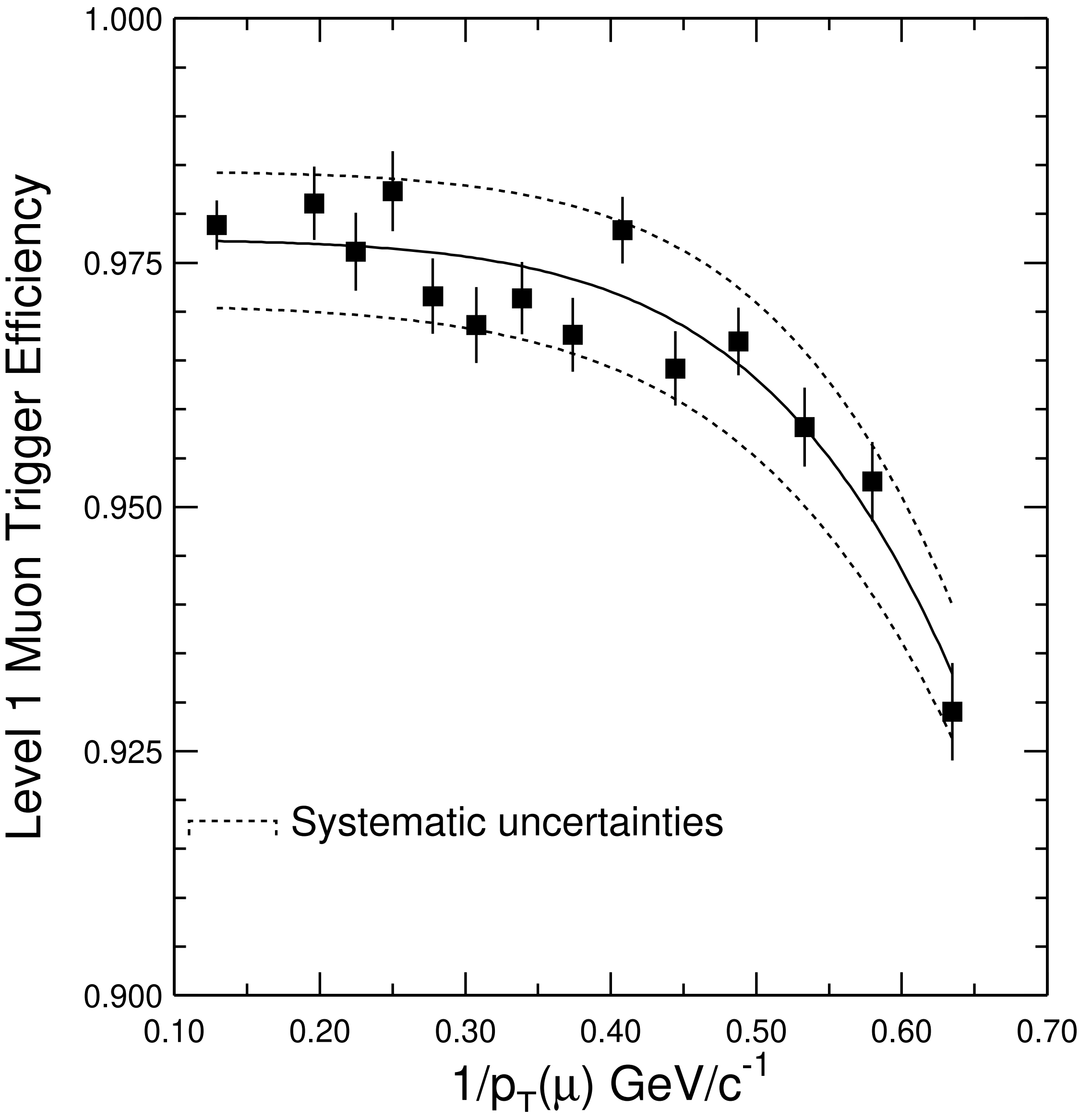

Figure 6: Fit to L1 CMU trigger efficiency data used in the cross-section measurement (solid line) and the range used to determine the uncertainty (dashed line).

To determine the uncertainty in the L1 trigger efficiency, while also taking into account the data fluctuations around the central fit as shown in Figure 6, the range of the uppermost and lowermost fluctuations supported by the data are computed as follows: $x'(p_T) = \bar{x} \pm (|x - \bar{x}| + 1\sigma)$ where x is the data value, $\bar{x}$ is the value returned by the fit and σ is the uncertainty on the data. The $x'(p_T)$ distribution is refit using the function in Equation 3. The results are shown as dashed lines in Figure 6 and are used to compute the uncertainty on the cross-section due to the L1 trigger efficiency measurement.

To calculate the J/ψ Level 1 trigger reconstruction efficiency taking into account $\mu - \mu$ co-relations, the Level 1 reconstruction efficiency of each J/ψ candidate in the J/ψ invariant mass region is measured:

$$\epsilon_{L1}^{J/\psi}(p_T^{J/\psi}) = \epsilon_{L1}^{\mu}(p_T^{\mu_1})\epsilon_{L1}^{\mu}(p_T^{\mu_2})$$

The mean and RMS of the Level 1 di-muon trigger efficiency distribution in each J/ψ transverse momentum bin is shown in Figure 7 and listed in the Table 4.

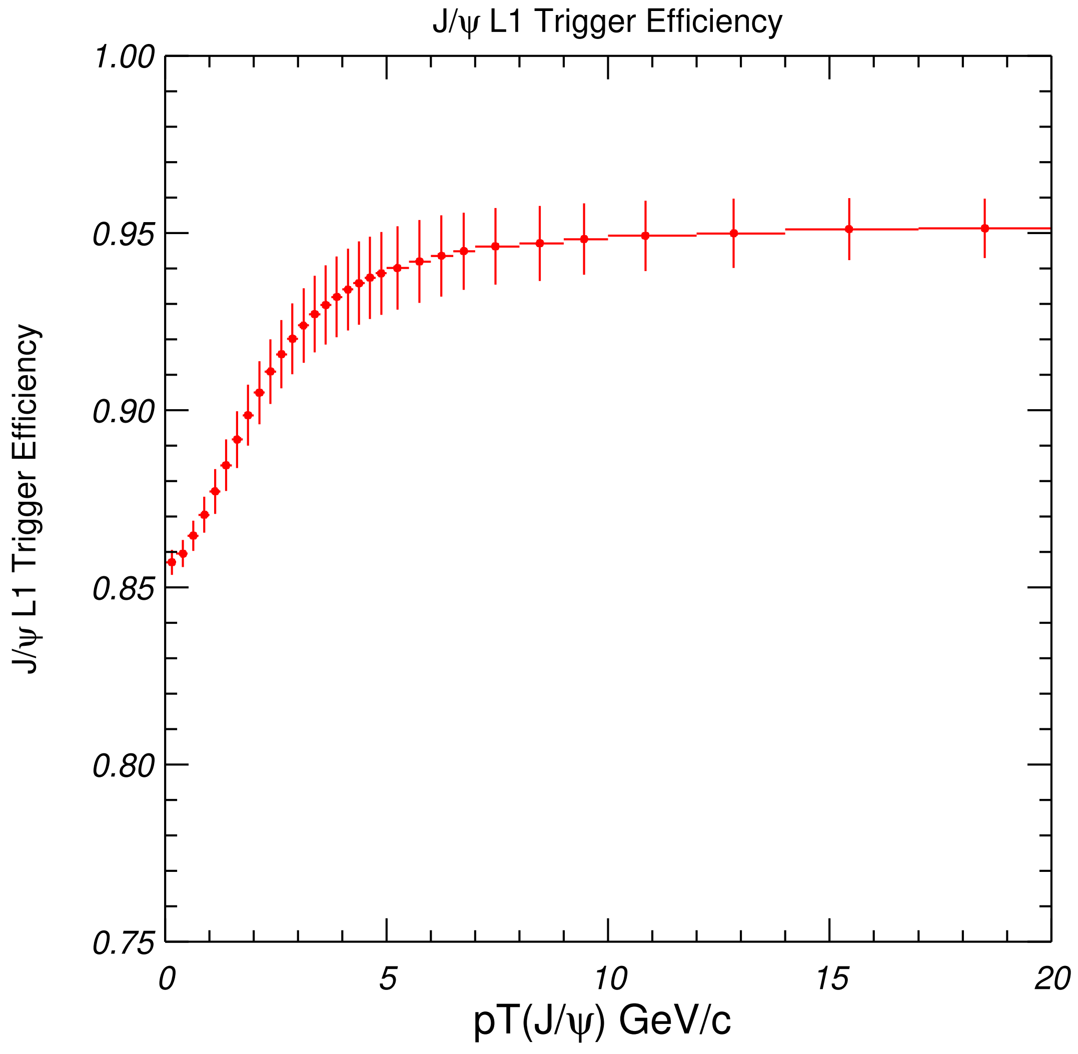

Figure 7: $J/\psi \to \mu\mu$ Level 1 trigger efficiency as a function of J/ψ transverse momenta. The points are the mean of the dimuon efficiency in each bin and the error bars are the RMS of the dimuon efficiency distribution.

$p_T(J/\psi)$ GeV/c	L1 Efficiency (MEAN)	RMS
$0.0 - 0.25$	0.8571	0.0035
$0.25 - 0.5$	0.8595	0.0038
$0.5 - 0.75$	0.8646	0.0042
$0.75 - 1.0$	0.8705	0.0050
$1.0 - 1.25$	0.8771	0.0063
$1.25 - 1.5$	0.8845	0.0072
$1.5 - 1.75$	0.8917	0.0080
$1.75 - 2.0$	0.8986	0.0086
$2.0 - 2.25$	0.9049	0.0089
$2.25 - 2.5$	0.9109	0.0091
$2.5 - 2.75$	0.9158	0.0096
$2.75 - 3.0$	0.920	0.010
$3.0 - 3.25$	0.924	0.010
$3.25 - 3.5$	0.927	0.010
$3.5 - 3.75$	0.930	0.011
$3.75 - 4.0$	0.932	0.011
$4.0 - 4.25$	0.934	0.011
$4.25 - 4.5$	0.936	0.011
$4.5 - 4.75$	0.937	0.011
$4.75 - 5.0$	0.939	0.011
$5.0 - 5.5$	0.940	0.011
$5.5 - 6.0$	0.942	0.011
$6.0 - 6.5$	0.946	0.011
$6.5 - 7.0$	0.945	0.010
$7.0 - 8.0$	0.946	0.010
$8.0 - 9.0$	0.947	0.010
$9.0 - 10.0$	0.948	0.010
$10.0 - 12.0$	0.9492	0.0099
$12.0 - 14.0$	0.9499	0.0097
$14.0 - 17.0$	0.9511	0.0087
$17 - 20.0$	0.9513	0.0083

Table 4: $J/\psi \rightarrow \mu\mu$ Level 1 trigger efficiency as a function of J/ψ transverse momenta.

4.2 Level 3 trigger reconstruction

The L3 reconstruction efficiency is dominated by the difference in the online and offline tracking efficiency. Only the Histogram-Linking (HL) algorithim is used for pattern recognition in the COT at Level 3. The merged HL and Segment-Linking (SL) algorithims are combined in offline reconstruction to give a higher overall COT tracking efficiency. Most offline tracks are reconstructed using the SL algorithim. In addition, the hit finding efficiency of the SL algorithim in version 4.8.4 has been improved. The L3 HL tracking algorithim and muon reconstruction algorithim used for the dataset considered is v4.3.0. The v4.3.0 L3 muon reconstruction efficiency

cut	J/ψ signal	sideband	net
$\lvert\Delta_z(\mu\mu)\rvert < 5$ cm	8453	2300	7303 ± 95
$\lvert\Delta_z(\mu\mu)\rvert >= 5$ cm	42	103	-9.5 ± 8.2

Table 5: Efficiency of L3 selection cut on the z seperation of the two muons from the J/ψ. Events found in the CMUP4 and CMUP8 single muon trigger samples.

measured relative to v4.8.4 of the COT and CMU offline reconstruction is discussed in detail in [9]. The L3 single muon reconstruction efficiency is found to be flat for $p_T(\mu) > 1.5$ GeV/c and is

$$\epsilon^{\mu}_{L3/Offline} = 0.997 \pm 0.001(stat) \pm 0.002(syst) \tag{4}$$

The efficiency of the L3 selection cut on the z seperation of the two muons from the J/ψ was measured using the J/ψs reconstructed in the single muon trigger samples [9]. The number of events that passed and failed the z seperation cut in the mass signal and sideband regions is listed in Table 5. The cut efficiency is:

$$\epsilon^{\mu\mu}_{\Delta_z} = \frac{N_{passed}}{N_{passed} + N_{failed}} = 1.0013 \pm 0.0011 \tag{5}$$

4.3 COT offline reconstruction

The COT tracking efficiency was measured using a Monte Carlo track embedding technique [21]. Monte Carlo μ tracks are embedded into CDF Run II di-muon events. The resolution scale factor and hit merging distance is adjusted such that the embedded track has residuals and hit distributions matched to μ-tracks in J/ψ data events. The efficiency of COT track reconstruction in di-muon events using the track embedding method was estimated to be

$$\epsilon_{COT}(p^{\mu}_T > 1.5\mathrm{GeV/c}) = 99.61 \pm 0.02(stat)^{+0.34}_{-0.91}(syst)\% \tag{6}$$

4.4 CMU Muon offline reconstruction

The muon reconstruction efficiency was studied by the muon reconstruction group [35]. J/ψs were reconstructed from the muon+SVT samples where the $J\psi$ is reconstructed from the triggered CMUP muon and the COT+SVXII track that triggered the SVT leg. The efficiency was calculated by projecting the SVT leg into the muon chambers and determining whether a muon is reconstructed when the track projection is within the CMU/UP/X fiducial volume. For CMU muons with transverse momenta > 1.5 GeV/c, the efficiency was found to be constant within measurement errors and was estimated to be [22]

$$\epsilon^{\mu}_{CMU} = 0.986 \pm 0.003 \pm 0.010 \tag{7}$$

All CMU wedges were included in this mearsurement. For the J/ψ cross-section measurement, wedge 17W which has an efficiency of ≈ 0.86 [22], is excluded. The remeasured CMU efficiency excluding 17W was found to be $\epsilon_{CMU} = 0.990 \pm 0.005 \pm 0.010$. The difference is smaller than the systematic uncertainty on the result recommended for the winter conferences.

To select clean CMU muons, the track-stub matching in the $r-\phi$ plane is required to have $\chi^2_{CMU}(\Delta r\phi) < 9$. The efficiency of this stub-track matching criteria has a small p_T^μ dependency:

$$\epsilon_{\chi^2} = (1.0018 \pm 0.0003) - (0.0024 \pm 0.0001)p_T^\mu \tag{8}$$

The efficiency of the $\chi^2_{CMU}(\Delta r\phi) < 9$ matching criteria as a function of $J/\psi \rightarrow \mu\mu$ transverse momenta, obtained using an event-by-event weighing is shown in Figure 8 and listed in Table 6. The systematic uncertainty on the weighed average matching cut efficiency is obtained by varying the normalization and slope in Equation 8 by one standard deviation. The change in the weighed average efficiency in each transverse momentum bin is found be $\leq 0.2\%$.

4.5 Summary of trigger and reconstruction efficiencies

The two muon stubs from the J/ψ are required to be seperated by two physical towers which have independant readout. Therefore, no correlation is expected in the muon reconstruction efficiencies of the two muons. For events with $p_T(J/\psi) < 5$ GeV/c, the 2 muon track opening angle in the $r-\phi$ plane is $\Delta\phi(two-track) > 30^0$, therefore the $\mu-\mu$ tracking efficiency correlations are negligible for that transverse momentum range. At higher transverse momenta the two-tower stub seperation requirement forces the 2 muon tracks to be seperated by at least 5^0, as a result the 2-track correlations are expected to be small. MC track embedding studies are being carried out to determine the size of the correlations. For the time being, the two μ-tracks are treated as uncorrelated in the estimation of the COT $J/\psi \rightarrow \mu\mu$ tracking reconstruction efficiency.

Since both muons originate from the same vertex, the efficiency of the track z_0 cut is 100% correlated and is counted only once. The combined p_T independant COT tracking, muon and L3 reconstruction efficiencies for CMU-CMU J/ψs is calculated to be

$$\epsilon_{rec} = \epsilon^2_{L3} \cdot \epsilon^2_{COT} \cdot \epsilon^2_{CMU} \cdot \epsilon_{z_0} \cdot \epsilon_{\Delta_z} = 95.5^{+2.1}_{-2.7}\% \tag{9}$$

A summary of all reconcstruction efficiencies to be considered is presented in Table 7

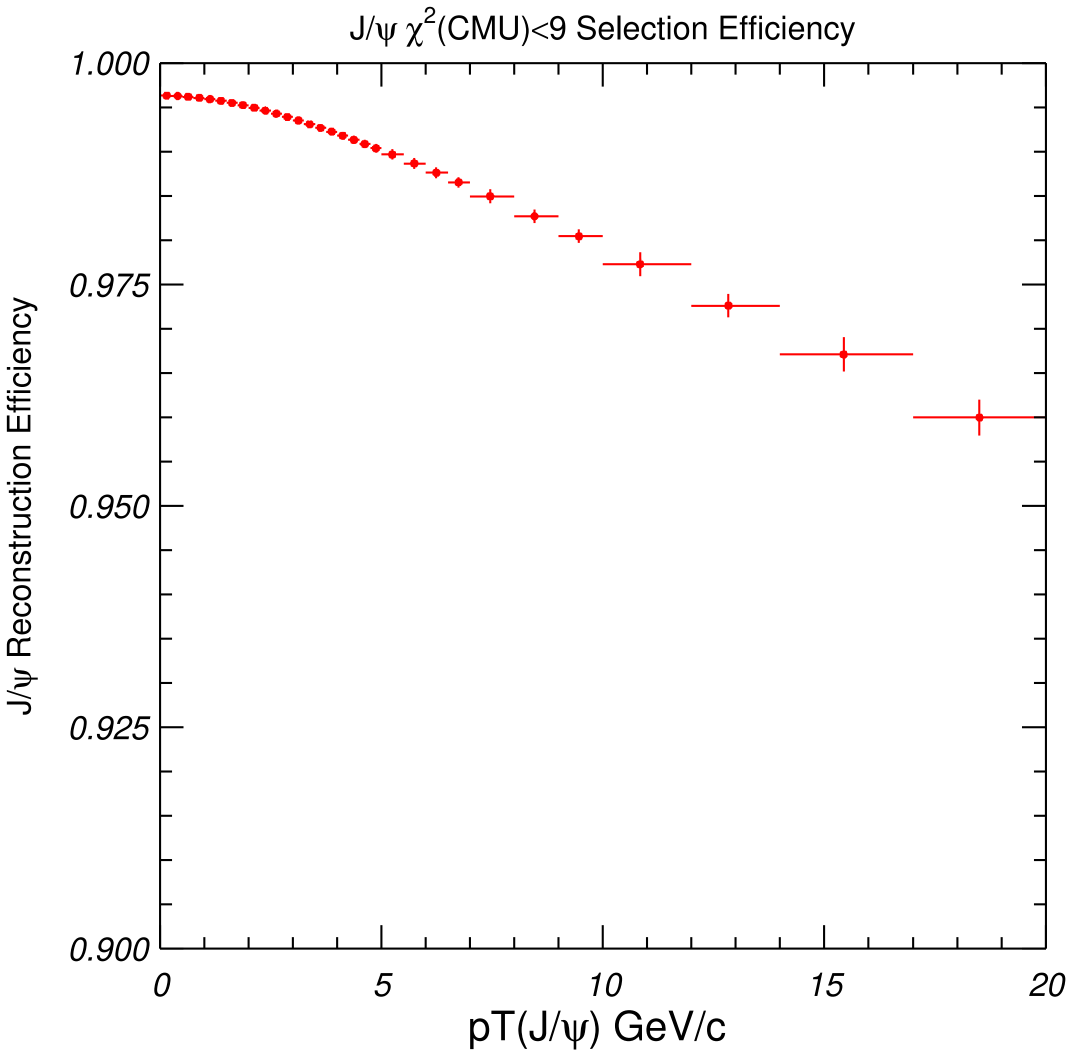

Figure 8: $J/\psi \to \mu\mu\ \chi^2_{CMU} < 9$ reconstruction efficiency as a function of J/ψ transverse momenta. The points are the mean of the dimuon efficiency in each bin and the error bars are the RMS of the dimuon efficiency distribution.

5 J/ψ Acceptance

Only a fraction of the J/ψ events produced in $p\bar{p}$ collision are collected and reconstructed by CDF due to its geometry and limited kinematic acceptances and its finite trigger and reconstruction efficiencies. We correct the observed number of events by the acceptances and efficiencies obtained using the following methods. The J/ψ online trigger efficiency and offline reconstruction performance have been discussed in the previous section.

The CMU muon detector covers the pseudo-rapidity range of $-0.6 < \eta < 0.6$ and

$p_T(J/\psi)$ GeV/c	$\chi^2_{CMU}(\Delta r\phi) < 9$ Efficiency (MEAN)	RMS
$0.0 - 0.25$	0.996327	0.000061
$0.25 - 0.5$	0.996282	0.000067
$0.5 - 0.75$	0.996193	0.000082
$0.75 - 1.0$	0.99608	0.00010
$1.0 - 1.25$	0.99593	0.00013
$1.25 - 1.5$	0.99573	0.00017
$1.5 - 1.75$	0.99551	0.00020
$1.75 - 2.0$	0.99525	0.00024
$2.0 - 2.25$	0.99496	0.00027
$2.25 - 2.5$	0.99463	0.00030
$2.5 - 2.75$	0.99429	0.00033
$2.75 - 3.0$	0.99391	0.00034
$3.0 - 3.25$	0.99352	0.00036
$3.25 - 3.5$	0.99310	0.00038
$3.5 - 3.75$	0.99268	0.00040
$3.75 - 4.0$	0.99225	0.00042
$4.0 - 4.25$	0.99180	0.00044
$4.25 - 4.5$	0.99133	0.00046
$4.5 - 4.75$	0.99086	0.00048
$4.75 - 5.0$	0.99038	0.00051
$5.0 - 5.5$	0.98967	0.00058
$5.5 - 6.0$	0.98866	0.00060
$6.0 - 6.5$	0.98761	0.00059
$6.5 - 7.0$	0.98653	0.00058
$7.0 - 8.0$	0.98496	0.00079
$8.0 - 9.0$	0.98270	0.00075
$9.0 - 10.0$	0.98044	0.00076
$10.0 - 12.0$	0.9772	0.0013
$12.0 - 14.0$	0.9726	0.0013
$14.0 - 17.0$	0.9671	0.0019
$17 - 20.0$	0.9600	0.0020

Table 6: $J/\psi \rightarrow \mu\mu$ $\chi^2_{CMU} < 9$ reconstruction efficiency as a function of J/ψ transverse momenta. Each point is the mean of the di-muon selection efficiency in the J/ψ bin and the RMS of the efficiency distribution in each bin is also listed.

is segmented in ϕ into 24 12.6^0 wedges with a 2.4^0 seperation between each wedge [23]. In this region the coverage of the central tracking chamber, COT is 100% and the CDF detector acceptance is driven by the muon detector geometry and kinematic reach. The calorimeter acts as an absorber for the CMU detector which is therefore only sensitive to muons with $p_T > 1.35$ GeV/c. The arrangement of the 4 sense wires within the CMU chambers allows a lower bound on the transverse momentum of the muon to be calculated from the difference in drift times in sense wires on

J/ψ Selection	Efficiency	Reference
L1/L3&Offline	$\epsilon^{\mu}_{L1} = (0.9774 \pm 0.0020) freq\left(\frac{(1.10\pm0.11)-1/p_T}{(0.276\pm0.060)}\right)$	CDFNOTE 6162
$\chi^2(\Delta r\phi)_{CMU} < 9$	$\epsilon_{\chi^2} = (1.0018 \pm 0.0003) - (0.0024 \pm 0.0001)p_T$	CDFNOTE 6114
L3&Offline/Offline	$\epsilon^{\mu}_{L3} = 99.7 \pm 0.1 \pm 0.2\%$	CDFNOTE 6144
COT Offline	$\epsilon_{COT}(p^{\mu}_T > 1.5\text{GeV/c}) = 99.61 \pm 0.02^{+0.34}_{-0.91}\%$	CDFNOTE 6394
Muon Offline	$\epsilon_{CMU} = 98.6 \pm 0.3 \pm 1.0\%$	CDFNOTE 6347
$z_0(\mu) < 90cm$	$\epsilon_{z0} = 99.43 \pm 0.16\%$	J/ψs muons
$\lvert z_{0_{\mu_1}} - z_{0_{\mu_2}}\rvert < 5$ cm	$\epsilon_{\Delta z} = 1.0013 \pm 0.0011\%$	D. Litvintsev
CMU fiducial	MC acceptance	this note
Exclude CMU 17W	MC acceptance	this note
2 tower seperation	MC acceptance	this note
SL2468	MC acceptance	this note
Matchbox 8	MC acceptance	this note
$\Delta\phi(\mu\mu) < 130^0$	MC acceptance	this note
$p_T(\mu) > 1.5$ GeV/c	MC acceptance	this note
$z_0(\mu) < 90cm$	MC correction	this note
$\lvert y\rvert < 0.6$	MC acceptance	this note
$\lvert\eta\rvert < 1.0$	MC acceptance	this note

Table 7: Summary of J/ψ trigger and offline reconstruction efficiencies. MC acceptance indicates that the combined efficiency of all the indicated cuts will be calculated from a MC simulation.

alternating layers. The CMU $\Delta T \leq 396ns$ timing window is selected such that it is fully efficient for muons with $p_T > 1.5GeV/c$ but CMU acceptance for muons with $1.5 < p_T < 1.7GeV/c$ is reduced due to range out in the calorimeter material.

To accurately model the acceptance of the CMU detector, firstly, the fiducial coverage needs to be modeled accurately, secondly, active regions of the detector with known hardware problems or low efficiencies need to be identified and modeled, and, thirdly, the range out of the muon track in the calorimeter material needs to be correctly modeled to determine the kinematic acceptance for low momentum muons.

The acceptance is calculated seperately for events from the two L3 trigger paths with different cuts on the opening angle of the dimuon. J/ψ events where either μ stub was reconstructed in 17W are excluded from the cross-section calculation and taken into account in the acceptance calculation.

5.1 Monte Carlo Simulation using GEANT

Monte Carlo simulation methods were used to estimate the geometric and kinematic acceptances. The MC sample used in previous versions of CDFNOTE 6288 to calculate the inclusive J/ψ cross-section from 2 - 17 GeV/c was generated flat in pT and $|\eta| < 1.0$ and reweighed to match the Run I pT spectrum extrapolated to 2 GeV/c.

We found that the reweighing was done incorrectly. The generated dimuon pT was used instead of the $J/\psi \rightarrow \mu\mu\gamma$ generated transverse momentum. A correction to the acceptance was therefore applied to the previous results at $p_T > 10 GeV/c$. Using the corrected differential cross-section data from CDFNOTE 6288, a fit to the initial results using the parameteric form:

$$\frac{d\sigma}{dp_T(J/\psi)} = \frac{A p_T^b}{(p_T^2 + m^2)^n} \tag{10}$$

is performed. We find that $A = 7300000$, $b = 1.02013$, $m = 4.19773$ and $n = 3.98338$. A new MC sample is generated using the parameterized $p_T(J/\psi)$ spectrum obtained above for all the studied range and with a flat distribution in *rapidity* $|y| < 0.6$ [5].

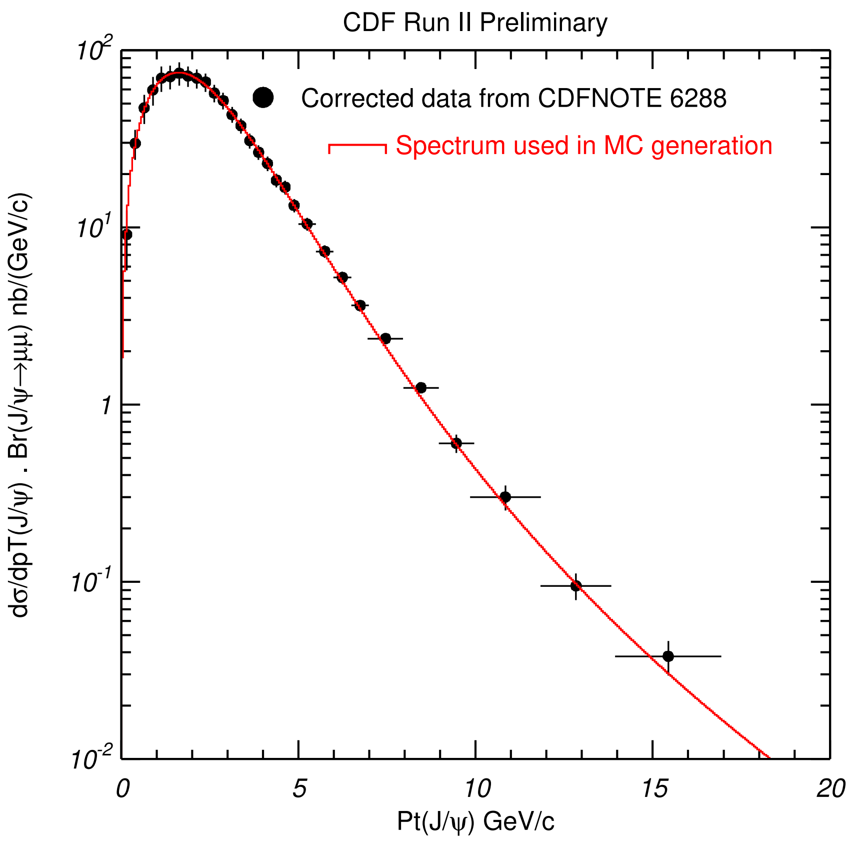

Figure 9: New MC spectrum

A full GEANT simulation of the CMU detector from v4.11.2 of the CDF simulation code is used to estimate the acceptance correction. Different data run numbers

[5]This is based on the Run II D0 results which indicate the inclusive cross-section is flat up to $|y| < 1.8$.

are used to simulate the primary vertex position and slopes in the GEANT sample generated as well as the SVXII coverage. The run numbers are selected to match the good data runs used in the analysis with the number of events per run weighted to match the integrated live luminosity.

The GEANT simulation was validated by comparing the distributions of various kinematic quantities in data and reconstructed MC events. The comparison between the MC and data distributions of p_T, η and $\Delta\phi(\mu\mu)$ are shown in Figure 10. The η distributions and the opening angle distributions in data and MC agree well when the p_T of the generated J/ψ models the data correctly. In Figure 11 it is shown that a good agreement is also obtained between the momentum distributions of the muon with the lowest and highest p_T in each event in data and MC. To validate the fiducial description of the muon chambers in the GEANT simulation, the μ track z co-ordinate is extrapolated to the CMU enterence radius of 347cm. A simple straight line extrapolation is used. The distribution of events in data and MC is shown in Figure 12. There are more events in the MC reconstructed in the region of the gap between the east and west arches than in the data. A systematic uncertainty on the acceptance will be assigned to account for this effect as discussed in section 5.2.

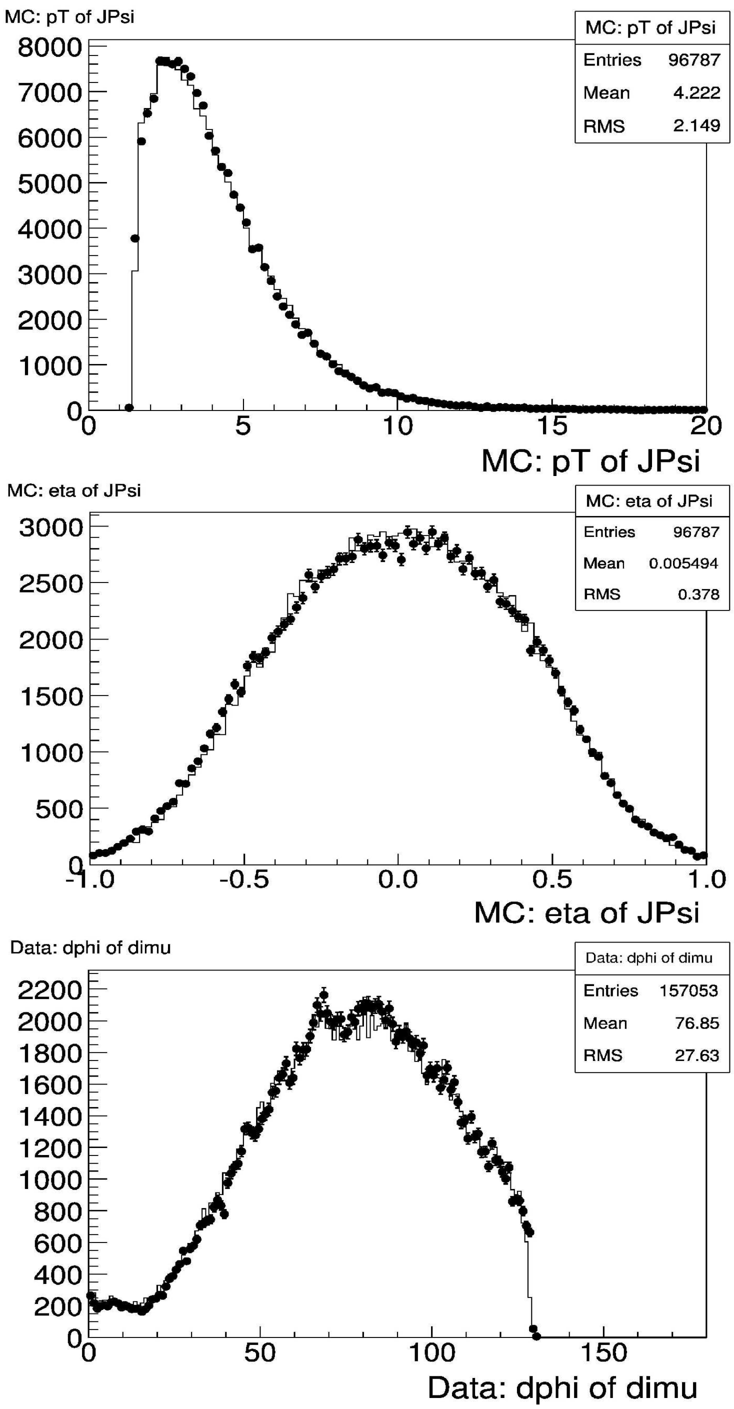

Figure 10: Data/MC comparison of the J/ψ transverse momentum, pseudo-rapdity and opening angle distributions. Histograms are GEANT MC from cdfsoft v4.9.1, black circles are data processed with cdfsoft v4.8.4. The J/ψ p_T in the MC was weighted to match the data.

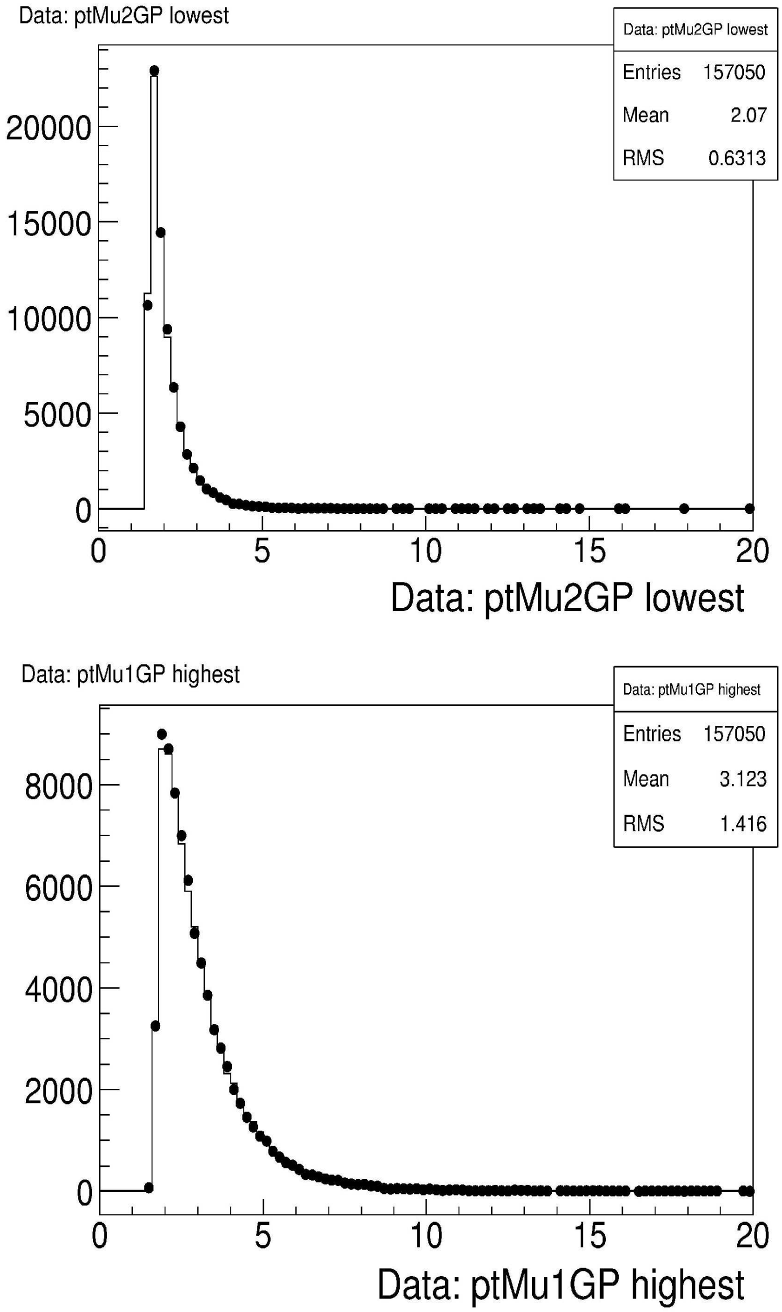

Figure 11: Data/MC comparison of the transverse momentum of both muons from J/ψ. Histograms are GEANT MC from cdfsoft v4.9.1, black circles are data processed with cdfsoft v4.8.4. The J/ψ p_T in the MC was weighted to match the data.

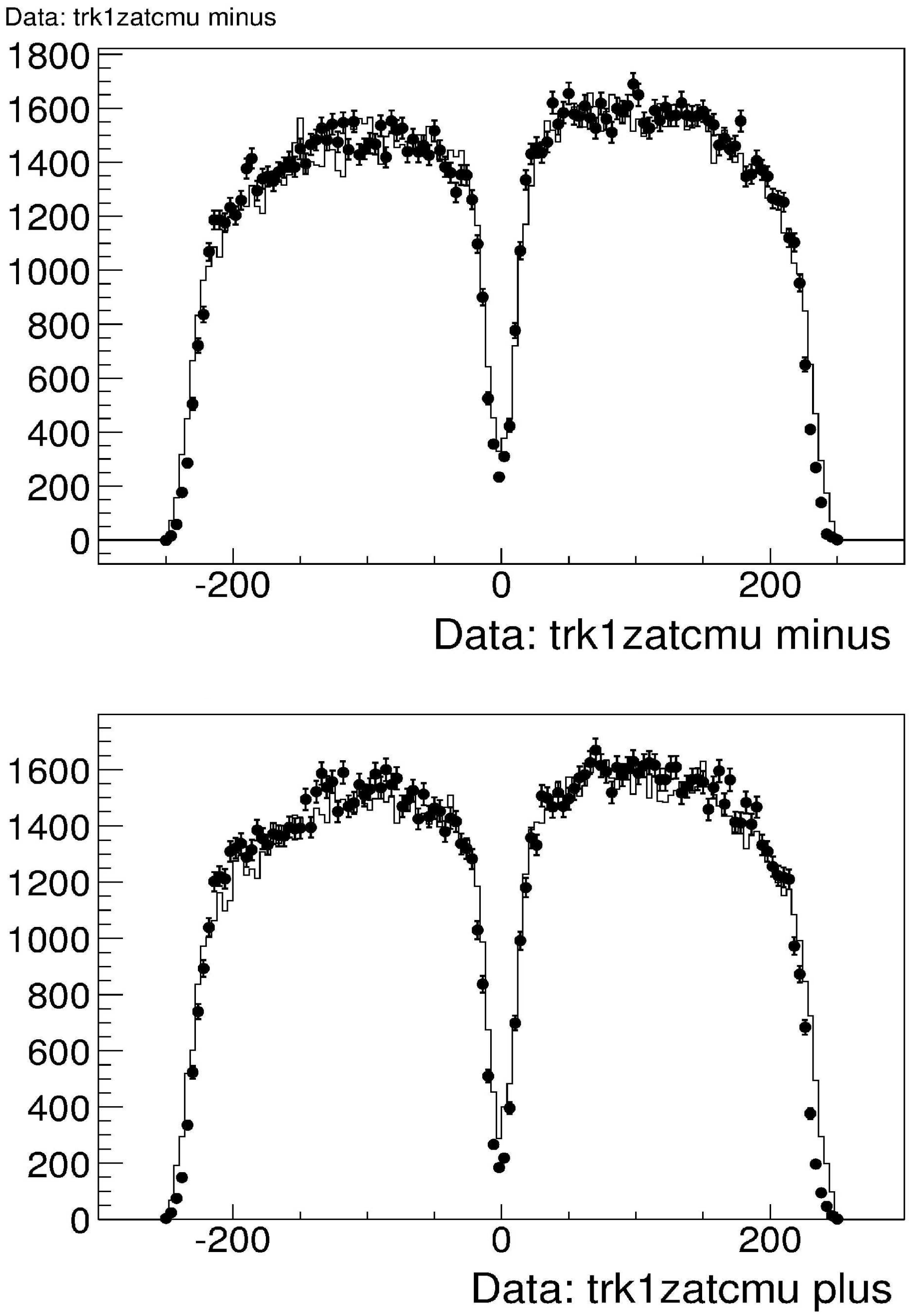

Figure 12: Data/MC comparison of the μ track z co-ordinate measured at $R = 347$ cm. Histograms are GEANT MC from cdfsoft v4.9.1, black circles are data processed with cdfsoft v4.8.4. COT only tracks is used.

The acceptance efficiency as a function of reconstructed $p_T(J/\psi)$ and rapidity, $y(J/\psi)$ is defined as

$$\mathcal{A}(p_T, y) = \frac{\#\ J/\psi(p_T(\mu\mu), |y| < 0.6, \mu_{type} = CMU, p_T(\mu) > 1.5, L1/L3/Offline\ cuts)}{\#\ J/\psi(p'_T(J/\psi), |y'| < 0.6)\ generated}$$

where $p'_T(J/\psi)$ and y' are the generated true values of the J/ψ momentum and rapidity including the radiated photon. The acceptance as a function of p_T and y is shown in Figure 13. As shown in Figure 13, the acceptance in the range 0.0-0.25 GeV/c is rapidly varying as a function of $p_T(J/\psi)$. A bin size of 50 MeV/c in p_T is therefore chosen to model the 2-D acceptance in the range 0-0.25 GeV/c.

5.2 Systematic uncertainties

J/ψ **production polarization** Kinematic acceptance depends on J/ψ polarization which populates the muon momentum spectrum differently. The Run-I published result on J/ψ polarization [28] [29] indicates all the polarization measurements for J/ψ are consistent with zero but could also be as large as 50% in some p_T regions. The polarization parameter α is such that the normalized angular distribution as a function of the angle θ between the μ in the J/ψ rest frame and the direction of the J/ψ in the lab frame is [28]:

$$I(\theta) = \frac{3}{2(\alpha + 3)}(1 + \alpha \cos^2 \theta)$$

. The values of α obtained from the Run I measurement are listed in Table 8

Pt bin	inclusive α	σ syst	σ total
4-5	0.236 ± 0.097	0.13	0.162
5-6	-0.001 ± 0.073	0.07	0.101
6-8	0.209 ± 0.054	0.04	0.067
8-10	0.266 ± 0.065	0.02	0.068
10-12	0.084 ± 0.084	0.02	0.086
12-15	0.14 ± 0.11	0.02	0.112
15-20	-0.30 ± 0.12	0.05	0.130

Table 8: Value of the inclusive J/ψ polarization parameter, α, measured in Run I

Taking the weighted mean from Table 8 and using the total error we get $\alpha = 0.134 \pm 0.0344$ were the error is the error on the mean value. The polarization is expected to decrease with lower transverse momenta and approach zero at $p_T = 0$. The following considerations were taken into account in determining the final value of $\sigma\alpha$ to use for the acceptance uncertainty:

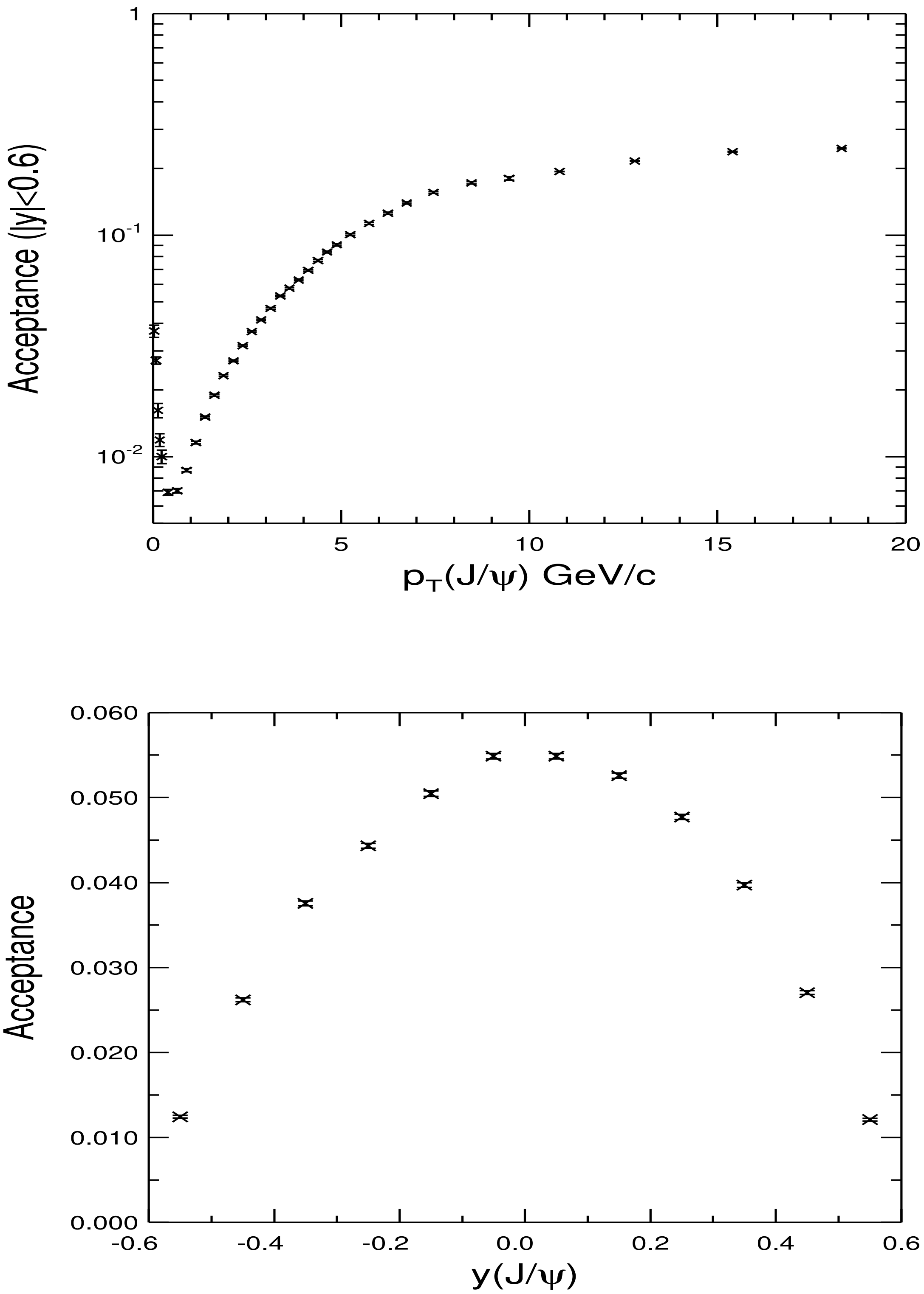

Figure 13: Acceptance of $J/\psi \to \mu\mu$ events measured using a GEANT simulation of the CDF II detector. The acceptance is shown as a function of $p_T(J/\psi)$ and $y(J/\psi)$.

1. We do not want to use a number that excludes zero at $p_T = 0$
2. The χ^2 per degree of freedom of a straight-line fit to the data is 3.13. That's not such a good fit.
3. The uncertainty on the lowest point, the point nearest the bulk of our low p_T data is 0.162.

Therefore the value of $\alpha = 0.13 \pm 0.15$ is used for the final acceptence values. The new acceptance values using the realistic input spectrum, and the uncertainty due to the polarization are recomputed and shown in Table 10. The uncertainty due to polarization is largest in the lower momentum bins and is around 5% near $p_T = 0$.

Generated $p_T(J/\psi)$ The acceptance is calculated in bins of y and p_T to minimize the uncertainty from the lack of knowledge of the J/ψ production spectrum. The acceptance obtained is a rapidly varying function of the J/ψ transverse momentum in the region of $0 - 0.25$ GeV/c (Figure 13). A 20% variation in the cross-section value in the range $0 - 0.25$ is observed when different p_T bin sizes are used to correct the observed event yields by the 2-D acceptance. As shown in Table 9 no significant variation in cross-section is observed when smaller bin sizes are used. Based on the study shown in Table 9, a bin size of 50 MeV/c is used to paramterize the 2-D MC distribution for the calculation of the cross-section in the 0 to 250 MeV/c J/ψ transverse momentum bin.

p_T bin size (MeV/c)	$d\sigma/dp_T$ from 0.0-0.25 GeV/c
50*	9.1
100	9.0
200	8.4
250	7.2

Table 9: Variation in the cross-section measured in the 0-0.25 GeV/c bin as a function of the p_T bin size used in the acceptance measurement. *This is the default bin size used.

The cross-section shape is first obtained using the acceptance from the default generated p_T distribution which matches the preliminary data cross-section distribution. To estimate the uncertainty on the acceptance from variations in the input transverse momentum spectrum, the MC is reweighed such that the p_T distribution is flat and the acceptance recalculated. The fractional change in acceptance is taken as the symmetric uncertainty on the input transverse momentum distribution. The uncertainty is around 5% in the lowest momentum bin and for momenta from 0.25 to 3 GeV/c the uncertainty is $\leq 1\%$. From 3-4 GeV/c the uncertainty is 1-2% and for 4 to 20GeV/c, we find the variation is within 2-4%. The uncertianty values assigned are listed in Table 10.

$p_T(J/\psi)$ GeV/c	Acceptance ($\alpha = 0.13$)	Polarization syst. uncert(%)	SVXII material uncert. (%)	Generated $p_T(J/\psi)$ uncert. (%)
$0.0 - 0.05$	$0.0369 \pm 0.0024*$	$+4.6 - 4.2$	$\pm3\%$	$\pm3\%$
$0.05 - 0.1$	$0.0272 \pm 0.0010*$	$4.6 - 4.2$	$\pm3\%$	$\pm5\%$
$0.1 - 0.15$	$0.0162 \pm 0.0012*$	$4.7 - 4.3$	$\pm3\%$	$\pm1\%$
$0.15 - 0.2$	$0.0119 \pm 0.0008*$	$4.9 - 4.4$	$\pm3\%$	$\pm0\%$
$0.2 - 0.25$	$0.0100 \pm 0.0007*$	$4.7 - 4.3$	$\pm3\%$	$\pm0\%$
$0.25 - 0.5$	$0.00691 \pm 0.00020*$	$4.8 - 4.4$	$\pm3\%$	$\pm1\%$
$0.5 - 0.75$	$0.00702 \pm 0.00016*$	$4.8 - 4.4$	$\pm2\%$	$\pm1\%$
$0.75 - 1.0$	$0.00869 \pm 0.00015*$	$4.8 - 4.4$	$\pm2\%$	$\pm0.4\%$
$1.0 - 1.25$	0.01158 ± 0.00016	$4.8 - 4.4$	$\pm2\%$	$\pm0.2\%$
$1.25 - 1.5$	0.01511 ± 0.00018	$4.7 - 4.3$	$\pm2\%$	$\pm0.0\%$
$1.5 - 1.75$	0.01895 ± 0.00020	$4.7 - 4.3$	$\pm1\%$	$\pm0.0\%$
$1.75 - 2.0$	0.02322 ± 0.00022	$4.6 - 4.2$	$\pm1\%$	$\pm0.2\%$
$2.0 - 2.25$	0.02708 ± 0.00025	$4.6 - 4.1$	$\pm0.4\%$	$\pm0.5\%$
$2.25 - 2.5$	0.03171 ± 0.00028	$4.5 - 4.1$	$\pm0.4\%$	$\pm0.6\%$
$2.5 - 2.75$	0.03667 ± 0.00031	$4.4 - 4.0$	$< 1\%$	$\pm0.8\%$
$2.75 - 3.0$	0.04147 ± 0.00035	$4.3 - 3.9$	$< 1\%$	$\pm1\%$
$3.0 - 3.25$	0.04672 ± 0.00040	$4.2 - 3.8$	$< 1\%$	$\approx 1\%$
$3.25 - 3.5$	0.05318 ± 0.00046	$4.1 - 3.7$	$< 1\%$	$\approx 1\%$
$3.5 - 3.75$	0.05761 ± 0.00052	$4.0 - 3.7$	$< 1\%$	$\approx 1\%$
$3.75 - 4.0$	0.06276 ± 0.00059	$3.9 - 3.5$	$< 1\%$	$\approx 2\%$
$4.0 - 4.25$	0.06942 ± 0.00067	$3.8 - 3.5$	$< 1\%$	$\approx 2\%$
$4.25 - 4.5$	0.07681 ± 0.00077	$3.7 - 3.4$	$< 1\%$	$\approx 2\%$
$4.5 - 4.75$	0.08396 ± 0.00087	$3.7 - 3.3$	$< 1\%$	$\approx 2\%$
$4.75 - 5.0$	0.09042 ± 0.00099	$3.6 - 3.3$	$< 1\%$	$\approx 2\%$
$5.0 - 5.5$	0.10055 ± 0.00084	$3.4 - 3.1$	$< 1\%$	$\approx 2\%$
$5.5 - 6.0$	0.1130 ± 0.0011	$3.3 - 3.0$	$< 1\%$	$\approx 2\%$
$6.0 - 6.5$	0.1257 ± 0.0013	$3.2 - 2.9$	$< 1\%$	$\approx 2\%$
$6.5 - 7.0$	0.1397 ± 0.0017	$3.0 - 2.9$	$< 1\%$	$\approx 2\%$
$7.0 - 8.0$	0.1561 ± 0.0016	$2.8 - 2.6$	$< 1\%$	$\approx 3\%$
$8.0 - 9.0$	0.1723 ± 0.0023	$2.7 - 2.4$	$< 1\%$	$\approx 3\%$
$9.0 - 10.0$	0.1807 ± 0.0032	$2.4 - 2.2$	$< 1\%$	$\approx 3\%$
$10.0 - 12.0$	0.1938 ± 0.0003	$2.1 - 1.9$	$< 1\%$	$\approx 3\%$
$12.0 - 14.0$	0.2163 ± 0.0006	$2.0 - 1.9$	$< 1\%$	$\approx 3\%$
$14.0 - 17.0$	0.2380 ± 0.0008	$\pm2\%$	$\pm2\%$	$\approx 4\%$
$17 - 20.0$	0.2465 ± 0.0015	$\pm2\%$	$\pm2\%$	$\approx 3\%$

Table 10: The p_T dependant J/ψ acceptance and systematic uncertainties.

y **smearing** The acceptance of CMU-CMU J/ψ as a function of y is shown in Figure 13. There is a small but non-zero acceptance at $|y| = 0.6$ due to detector resolution and the primary vertex smearing in z. J/ψ MC events generated with $|y| < 0.8$ are simulated. The relative acceptance of events generated with $|y| > 0.6$ and reconstructed with $|y| < 0.6$, $\mathcal{A}'$, is calculated thus:

$$\mathcal{A}'(p_T) = \frac{\#\ accepted\ J/\psi(|y|_{generated} > 0.6, |y|_{reconstructed} < 0.6)}{Total\ \#\ J/\psi(|y|_{generated} < 0.6)} \tag{11}$$

Of a MC sample of 226650 accepted J/ψs ($p_T > 2.0GeV/c$) with reconstructed $|y|_{reco} < 0.6$, 226488 of them were generated with $|y|_{gen} < 0.6$. The value of $\mathcal{A}'$ for all reconstructed events is therefore very small: $\mathcal{A}' = 0.00071 \pm 0.00006(stat)$. A correction factor of $(1 - \mathcal{A}') = 99.93\%$ is applied to the J/ψ yield calculated in each $p_T(J/\psi)$ bin.

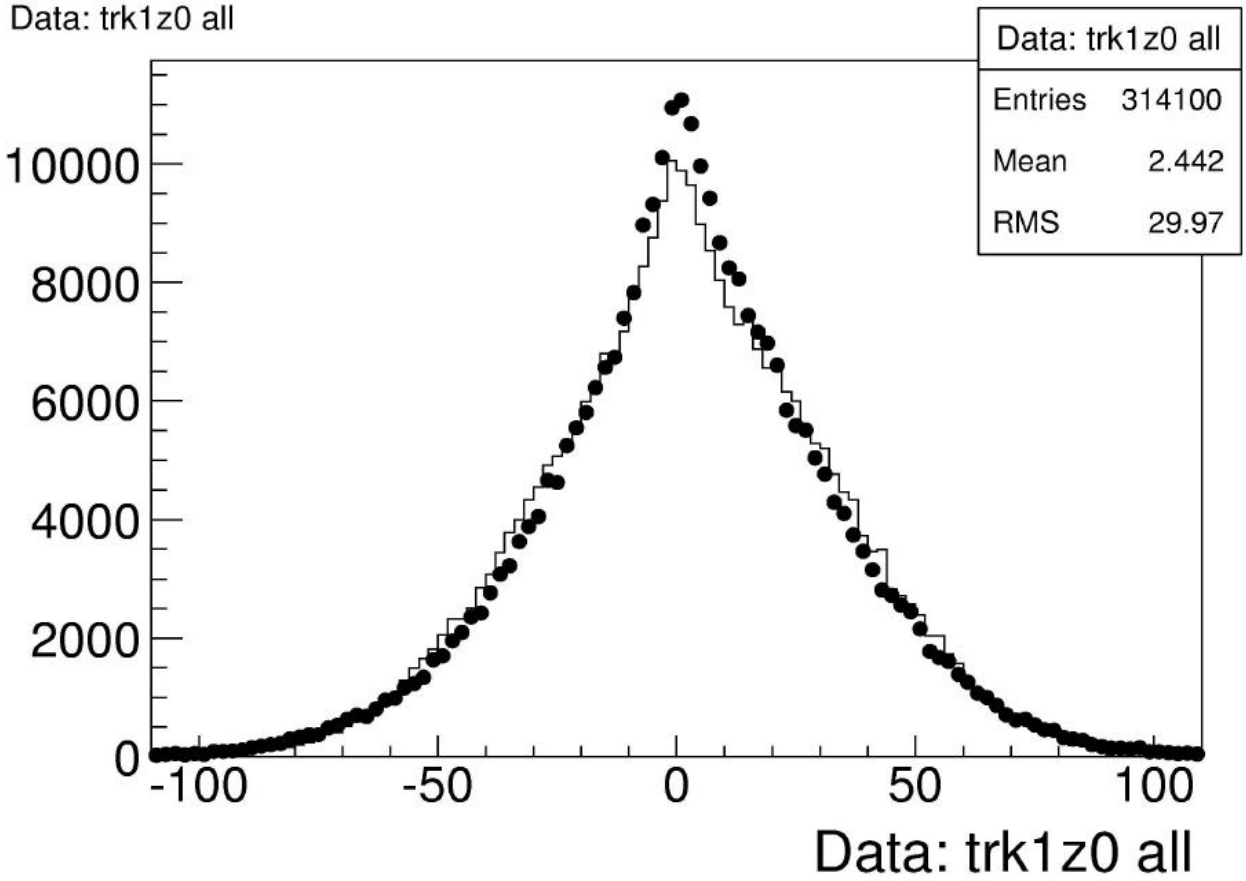

Figure 14: Data/MC comparison of the μ track z_0 co-ordinate Histograms are GEANT MC from cdfsoft v4.9.1, black circles are data processed with cdfsoft v4.8.4.

Primary vertex simulation CMU Muons from J/ψ are required to have $|z_0| < 90$ cm. As shown in Figure 14, there is disagreement between data and the MC $z_0(\mu)$ distribution due to inadequate modeling of the interaction region in the MC simulation. The systematic error is estimated from the difference in the ratio of data and MC tracks with $|z_0| < 90cm$ compared to all CMU muons. We find an uncertainty of 0.28%.

CMU z gap A systematic uncertainty is assigned to account for the improper modeling of the size of the gap between the east and west arches. The scatter of μ tracks near the center of the detector in the calorimter material determines the fraction of events accepted by the CMU in the $|z|_{at\ CMU} \pm 20cm$ region. The fraction of data and MC events falling in the gap region as shown in Figure 12 is compared in data and MC. The deviation between the ratios in data and MC is taken as the uncertainty from the modeling of the CMU z fiducial volume. The measured uncertainty from the knowledge of the size of the east and west gaps is 0.20%.

CMU East-West asymmetry Several factors contribute to the difference in the number of observed J/ψ μ in the east and west portions of the detector. These include the shift in the primary vertex towards +ve z (east), the exclusion of wedge 17W and the uncertainty in the modeling of the z extent of the CMU detector, as well as the differences in the east and west chambers. The east-west acceptance asymmetry in the CMU detector is defined as:

$$Asym_{E-W} = \frac{N(\mu)_{east} - N(\mu)_{west}}{N(\mu)_{east} + N(\mu)_{west}}$$

where $N(\mu)_{east,west}$ is the number of muons reconstructed in the east and west portions of CMU respectively. The uncertainty in the modeling of the east and west CMU portions is defined as

$$\Delta_{E-W} = Asym^{Data}_{E-W} - Asym^{GEANT}_{E-W} = 0.80\%$$

CMU wedge-wedge variations The ϕ acceptance of the CMU detector obtained from the GEANT simulation does not correctly model differences in gain and efficiencies between wedges. The number of events reconstructed in each wedge in data and MC is shown in Figure 15 where the total number of events in MC is normalized to match the data.

Although we expect to see 10% fewer events in wedge 6E as predicted by the MC due to the smaller z fiducial volume (active volume is from z = -11cm to -206cm.) we do not see a reduction in relative acceptance in the data. This

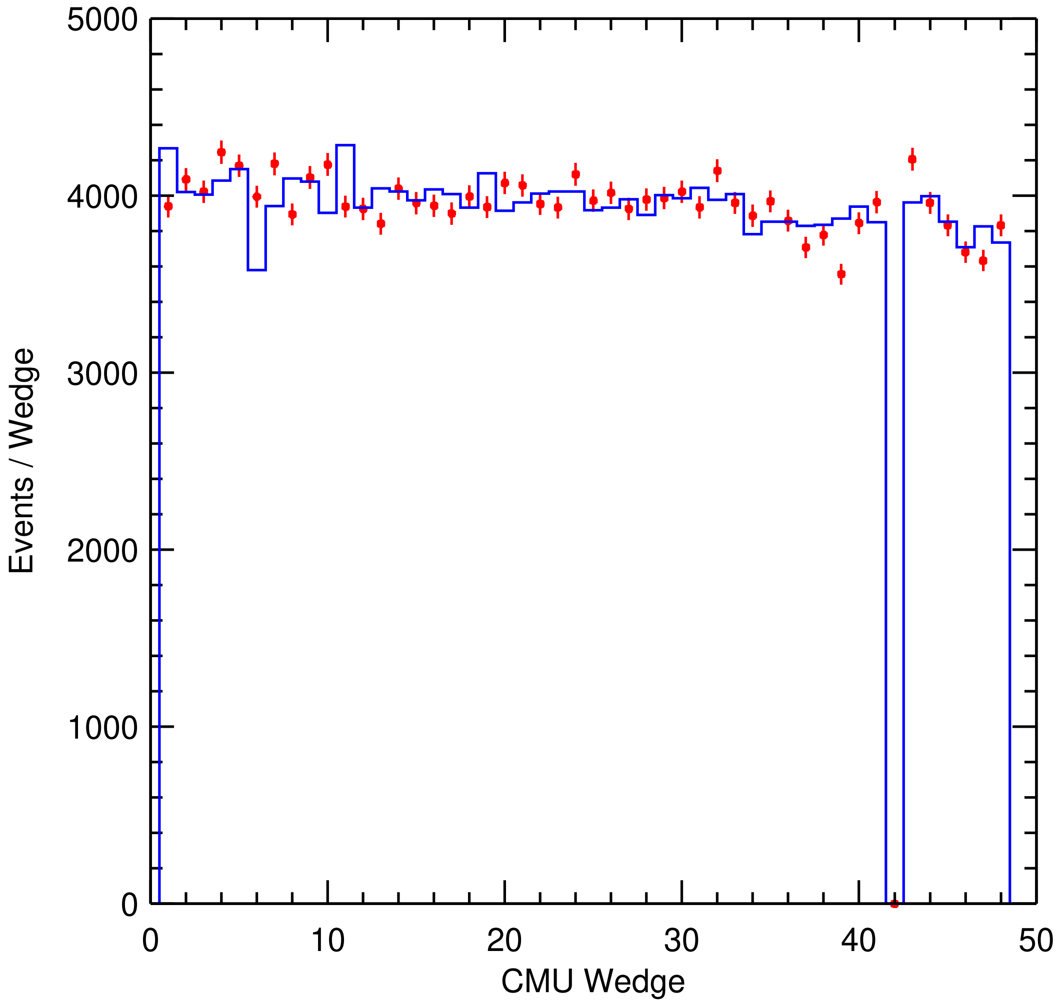

Figure 15: Data/MC comparison of the number of events in each of the 48 muon wedges. The total number of events in the MC is normalized to data. Wedges on the east are numbered 0-23 and wedges on the west are numbered from 24-47. Histograms are GEANT MC from cdfsoft v4.9.1, black circles are data processed with cdfsoft v4.8.4.

could be attributed to higher gain or efficiency in this wedge. The standard deviation of the difference in number of events reconstructed in each wedge in data and MC is taken as the uncertainty on the GEANT CMU ϕ acceptance. We find an overall uncertainty of 0.55%.

Energy loss in SVXII Material The SVXII material in v4.9.1 of GEANT is known to be incorrect. Its estimated that about $10-15\%$ of the SVXII material is unaccounted for in the current simulation. The distribution of this missing material is unknown, and the 4.9.1 version of the SiliMap material map overestimated the material in the central region by up to 10%. This introduces an uncertainty in the momentum resolution. The effect on the acceptance is greater at low J/ψ transverse momenta. To estimate the uncertainty on the acceptance from the incorrect accounting of the total energy loss in the SVXII detector, the SVXII material used in the parameteric simulation was reduced by 10% and increased by 20%, the systematic uncertainty is the difference between the acceptance values measured with different material scale factors and the nominal (nominal scale factor is 1.1). The results are listed in Table 10. The uncertainty is largest in the low momentum bins where it is around 5%.

Calorimeter Material The acceptance calculation of low momentum CMU muons is dependant on the accuracy with which range out in the calorimeter material is simulated in v4.9.1 GEANT. The central calorimeter and the muon absorber material are understood to be correctly modeled therefore no systematic uncertainty is assigned.

The total systematic error from the CMU fiducial volume and z vertex smearing is found to be 1.4% which is much smaller than the uncertainties from the lack of knowledge of the J/ψ production and decay kinematics such as polarization and the transverse momentum spectrum.

6 Cross Section Results

The J/ψ yield in each p_T bin is corrected for the 2-D acceptance, $\mathcal{A}(p_T^{J/\psi}, y^{J/\psi})$, L1 single muon trigger efficiency, $\epsilon_{L1}(p_T^{\mu})$, and the stub-track matching cuts, $\epsilon_{\chi^2<9}(p_T^{\mu})$, using an event by event weighing such that:

$$N(p_T)_{corrected} = \sum_{i=0}^{i=N_s} \frac{1}{w_i}$$

$$w_i = \epsilon_{L1}(p_T^{\mu 1}) \cdot \epsilon_{L1}(p_T^{\mu 2}) \cdot \epsilon_{\chi^2<9}(p_T^{\mu 1}) \cdot \epsilon_{\chi^2<9}(p_T^{\mu 1}) \cdot \mathcal{A}(p_T^{J/\psi}, y^{J/\psi})$$

where N_s is the number of signal events obtained from a fit to the invariant mass distribution of the reweighed events, using the same shapes for signal and background as shown in Figure 5. The error on the number of events in each inv. mass bin is given by:

$$\delta(N(p_T)) = \sqrt{\sum_{i=0}^{i=N_s} \left(\frac{1}{w_i}\right)^2}$$

In a similar fashion, the di-muon p_T distribution in each bin is reweighed. The corrected p_T distribution of the mass sideband subtracted events in the J/ψ mass region is used to determine the mean p_T value for each bin.

The J/ψ differential cross section is then calculated as follows:

$$\frac{d\sigma(p\bar{p} \to J/\psi X) \cdot Br(J/\psi \to \mu^+\mu^-)}{dp_T} = \frac{N(p_T)_{corrected} \cdot (1 - \mathcal{A}')}{\epsilon_{rec} \cdot \int Ldt \cdot \Delta p_T}$$

where $\sigma(J/\psi) \equiv \sigma(p\overline{p} \to J/\psi X, \mid y(J/\psi) \mid < 0.6)$, $\mathcal{A}'$ is the correction factor for y smearing, ϵ_{rec} is the combined L3, offline tracking and muon reconstruction efficiency, $\int Ldt$ is the integrated luminosity, and Δp_T is the bin size of the p_T bin. A source of p_T dependent systematic errors is the uncertainty on the L1 trigger low p_T muon efficiency given by Equation 3 and shown in . The cross-section is recalculated using the variation in the Level 1 single muon trigger efficiency shown in Figure 6. The Level 1 trigger uncertainties in each p_T bin are listed in Table 11. We find the bin-to-bin variations in the uncertainty to be small, therefore we assign a fully correlated uncertainty of $\pm 1.5\%$ from the L1 trigger efficiency to the inclusive cross-section measurement.

The cross-section values obtained with statistical and p_T dependent uncertainties are listed in Table 12.

The $+0.1\%$ systematic uncertainty on the measurement of the momentum scale discussed in Section 2.2 corresponds to an uncertainty of $d^2\sigma/dp_T^2 \times 0.1\%$ on the differential cross-section measured in each bin. Using the numbers in Table 12, the second derivative of the differential cross-section is calculated and the momentum scale uncertainty on the cross-section in each bin estimated. The effect was found to be small, the largest negative deviation being -0.08% and the largest positive deviation being +0.7%.

Table 13 summarizes the different contributions to the systematic errors to be applied to the cross-section measurement.

The differential crossection results are displayed in Figure 16. The invariant cross-section, $d\sigma/dp_T^2$ with systematic errors is shown in Figure 17. The mass sideband subtracted p_T^2 distribution is examined in each p_T bin; the mean of the distribution is used as the central value of p_T^2 in that range. The numbers are tabulated in Table 12.

The integrated cross section obtained from an integral of the differential cross section is:

$$\sigma(J/\psi) \equiv \sigma(p\overline{p} \to J/\psi X, p_T(J/\psi), \mid y(J/\psi) \mid < 0.6) = 240 \pm 1(stat) \pm 21(syst) \text{ nb}$$

The uncorrelated statistical errors are added in quadrature. The p_T dependent systematic uncertainties are added together and then added in quadrature with the correlated uncertainty of 7.0%:

$$\epsilon_{tot\ \sigma.Br}^{stat} = \sqrt{\sum_{i=1}^{i=N_{bins}} (\epsilon_i^{stat})^2} = 1.3 \tag{12}$$

$p_T(J/\psi)$ (GeV/c)	L1 Trigger syst.
$0.0 - 0.25$	$1.23 - 1.49\%$
$0.25 - 0.5$	$1.27 - 1.51\%$
$0.5 - 0.75$	$1.30 - 1.54\%$
$0.75 - 1.0$	$1.35 - 1.56\%$
$1.0 - 1.25$	$1.40 - 1.58\%$
$1.25 - 1.5$	$1.46 - 1.60\%$
$1.5 - 1.75$	$1.50 - 1.61\%$
$1.75 - 2.0$	$1.54 - 1.62\%$
$2.0 - 2.25$	$1.56 - 1.62\%$
$2.25 - 2.5$	$1.58 - 1.62\%$
$2.5 - 2.75$	$1.58 - 1.61\%$
$2.75 - 3.0$	$1.58 - 1.60\%$
$3.0 - 3.25$	$1.58 - 1.59\%$
$3.25 - 3.5$	$1.58 - 1.58\%$
$3.5 - 3.75$	$1.57 - 1.57\%$
$3.75 - 4.0$	$1.56 - 1.56\%$
$4.0 - 4.25$	$1.56 - 1.55\%$
$4.25 - 4.5$	$1.55 - 1.55\%$
$4.5 - 4.75$	$1.54 - 1.54\%$
$4.75 - 5.0$	$1.54 - 1.53\%$
$5.0 - 5.5$	$1.53 - 1.52\%$
$5.5 - 6.0$	$1.52 - 1.51\%$
$6.0 - 6.5$	$1.51 - 1.50\%$
$6.5 - 7.0$	$1.50 - 1.50\%$
$7.0 - 8.0$	$1.48 - 1.49\%$
$8.0 - 9.0$	$1.48 - 1.48\%$
$9.0 - 10.0$	$1.46 - 1.47\%$
$10.0 - 12.0$	$1.45 - 1.46\%$
$12.0 - 14.0$	$1.44 - 1.45\%$
$14.0 - 17.0$	$1.43 - 1.44\%$
$17 - 20.0$	$1.36 - 1.44\%$

Table 11: The fractional difference in the differential J/ψ cross-section as a function of p_T when the L1 trigger efficiency parameterization is varied.

$$\epsilon^{syst}_{tot\ \sigma.Br} = \left\{ \sum_{i=1}^{i=N_{bins}} \epsilon^{syst}_i(p_T) \right\} \oplus \pm 16 =^{+21}_{-19} \tag{13}$$

where N_{bins} is the total number of p_T bins, ϵ^{stat}_i is the statistical uncertainty in the cross-section measurement in the i^{th} bin, and $\epsilon^{syst}_i(p_T)$ is the systematic uncertainty on the measurement in each p_T bin independant of the the correlated systematic uncertainty of 7.0%.

$p_T(J/\psi)$ (GeV/c)	Mean p_T (p_T^2)	$\frac{d\sigma}{dp_T}\cdot\mathcal{B}$ (nb/GeV/c)	$\frac{d\sigma}{dp_T^2}\cdot\mathcal{B}$ (nb. GeV/c^{-2})
$0.0-0.25$	0.15(0.027)	$9.13\pm0.6^{+1.1}_{-0.7}*$	$36.5\pm2.4^{+4.2}_{-2.6}$
$0.25-0.5$	0.39(0.16)	$28.1\pm1.5^{+2.4}_{-1.6}*$	$37.4\pm2.0^{+3.1}_{-2.0}$
$0.5-0.75$	0.64(0.42)	$45.3\pm1.9^{+3.0}_{-2.1}*$	$36.2\pm1.5^{+2.5}_{-1.8}$
$0.75-1.0$	0.89(0.79)	$59.3\pm2.0^{+4.0}_{-2.9}*$	$33.9\pm1.1^{+2.3}_{-1.6}$
$1.0-1.25$	1.13(1.29)	$69.6\pm1.9^{+3.6}_{-3.2}$	$31.0\pm0.8^{+1.7}_{-1.5}$
$1.25-1.5$	1.38(1.91)	$73.4\pm1.7^{+3.9}_{-3.5}$	$26.7\pm0.6^{+1.4}_{-1.3}$
$1.5-1.75$	1.63(2.66)	$75.2\pm1.6^{+3.8}_{-3.3}$	$23.2\pm0.5^{+1.2}_{-1.0}$
$1.75-2.0$	1.87(3.52)	$72.9\pm1.4^{+3.7}_{-3.3}$	$19.4\pm0.4^{+0.9}_{-0.8}$
$2.0-2.25$	2.13(4.53)	$69.1\pm0.8^{+3.3}_{-2.9}$	$16.3\pm0.2^{+0.8}_{-0.7}$
$2.25-2.5$	2.38(5.65)	$67.3\pm1.0^{+3.1}_{-2.8}$	$14.2\pm0.2^{+0.7}_{-0.6}$
$2.5-2.75$	2.62(6.89)	$57.6\pm0.9^{+2.6}_{-2.4}$	$11.0\pm0.2^{+0.5}_{-0.5}$
$2.75-3.0$	2.87(8.26)	$52.0\pm0.8^{+2.4}_{-2.2}$	$9.04\pm0.13^{+0.41}_{-0.37}$
$3.0-3.25$	3.12(9.76)	$43.6\pm0.7^{+1.9}_{-1.8}$	$6.97\pm0.10^{+0.31}_{-0.28}$
$3.25-3.5$	3.38(11.4)	$37.3\pm0.6^{+1.6}_{-1.5}$	$5.53\pm0.08^{+0.24}_{-0.22}$
$3.5-3.75$	3.62(13.1)	$31.5\pm0.5^{+1.3}_{-1.2}$	$4.34\pm0.07^{+0.18}_{-0.17}$
$3.75-4.0$	3.87(15.0)	$26.2\pm0.4^{+1.2}_{-1.1}$	$3.38\pm0.05^{+0.15}_{-0.14}$
$4.0-4.25$	4.12(17.0)	$22.5\pm0.4^{+1.0}_{-0.9}$	$2.72\pm0.05^{+0.12}_{-0.11}$
$4.25-4.5$	4.38(19.2)	$18.7\pm0.3^{+0.8}_{-0.8}$	$2.13\pm0.04^{+0.09}_{-0.09}$
$4.5-4.75$	4.62(21.4)	$16.1\pm0.3^{+0.7}_{-0.6}$	$1.74\pm0.03^{+0.08}_{-0.07}$
$4.75-5.0$	4.88(23.8)	$13.3\pm0.3^{+0.6}_{-0.5}$	$1.37\pm0.03^{+0.06}_{-0.05}$
$5.0-5.5$	5.24(27.5)	$10.3\pm0.15^{+0.42}_{-0.40}$	$0.984\pm0.014^{+0.040}_{-0.038}$
$5.5-6.0$	5.74(33.0)	$7.28\pm0.12^{+0.29}_{-0.28}$	$0.633\pm0.010^{+0.025}_{-0.024}$
$6.0-6.5$	6.24(38.9)	$5.11\pm0.09^{+0.20}_{-0.19}$	$0.408\pm0.0069^{+0.016}_{-0.015}$
$6.5-7.0$	6.74(45.5)	$3.54\pm0.07^{+0.13}_{-0.14}$	$0.262\pm0.0052^{+0.010}_{-0.010}$
$7.0-8.0$	7.45(55.7)	$2.27\pm0.03^{+0.10}_{-0.09}$	$0.151\pm0.0019^{+0.006}_{-0.006}$
$8.0-9.0$	8.46(71.6)	$1.14\pm0.02^{+0.05}_{-0.05}$	$0.0668\pm0.0011^{+0.0028}_{-0.0027}$
$9.0-10.0$	9.46(89.5)	$0.622\pm0.013^{+0.025}_{-0.024}$	$0.0327\pm0.0007^{+0.0013}_{-0.0013}$
$10.0-12.0$	10.8(118)	$0.278\pm0.006^{+0.011}_{-0.010}$	$0.0126\pm0.0003^{+0.0005}_{-0.0005}$
$12.0-14.0$	12.8(165)	$0.103\pm0.003^{+0.004}_{-0.004}$	$0.00398\pm0.00013^{+0.00015}_{-0.00015}$
$14.0-17.0$	15.2(233)	$0.037\pm0.002^{+0.002}_{-0.002}$	$0.00120\pm0.00005^{+0.00006}_{-0.00006}$
$17-20.0$	18.3(336)	$0.014\pm0.001^{+0.001}_{-0.001}$	$0.00037\pm0.00004^{+0.00002}_{-0.00002}$

Table 12: The differential J/ψ crossection as a function of p_T, for $|y(J/\psi)| < 0.6$. For each measurement, the first uncertainty is statistical and the second uncertainty is the systematic. The systematic uncertainties shown are the p_T dependent uncertainties only. The fully correlated p_T independent systematic uncertainty in each bin is 7%.

6.1 Comparison with Run I

The integrated crossection for $p_T(J/\psi) > 5.0$ GeV/c in Run II is

$$\sigma(p\overline{p} \to J/\psi X, p_T(J/\psi) > 5.0GeV/c, \mid y(J/\psi) \mid < 0.6)_{RunII} = 18.1 \pm 0.1(stat) \pm 1.5(syst) \text{ nb}$$

From MC studies, the integrated cross-section of J/ψ with $p_T > 5$ GeV/c and $|y| < 0.6$ is found to be 10% higher than the cross-section over the same p_T range but for

Source	Systematic uncertainty
J/ψ Polarization	$\pm 2-5\%$ (p_T dependent)
J/ψ Spectrum	$\pm 0-5\%$ (p_T dependent)
SVXII material	$\pm 0.4-3\%$ (p_T dependent)
Mass fits	-1.3% *to* $+9\%$ (p_T dependent)
Momentum scale	-0.1% *to* $+0.7\%$ (p_T dependent)
Luminosity	$\pm 5.9\%$
Reconstruction eff.	$+2.1$ -2.7%
Detector simulation	$\pm 1.4\%$
Data quality	$\pm 1.0\%$
L1 trigger efficiency	$\pm 1.5\%$
Total	$\pm 7.0\% \oplus \epsilon(p_T^{J/\psi})$

Table 13: Sources of systematic uncertainties in the inclusive J/ψ cross-section measurement

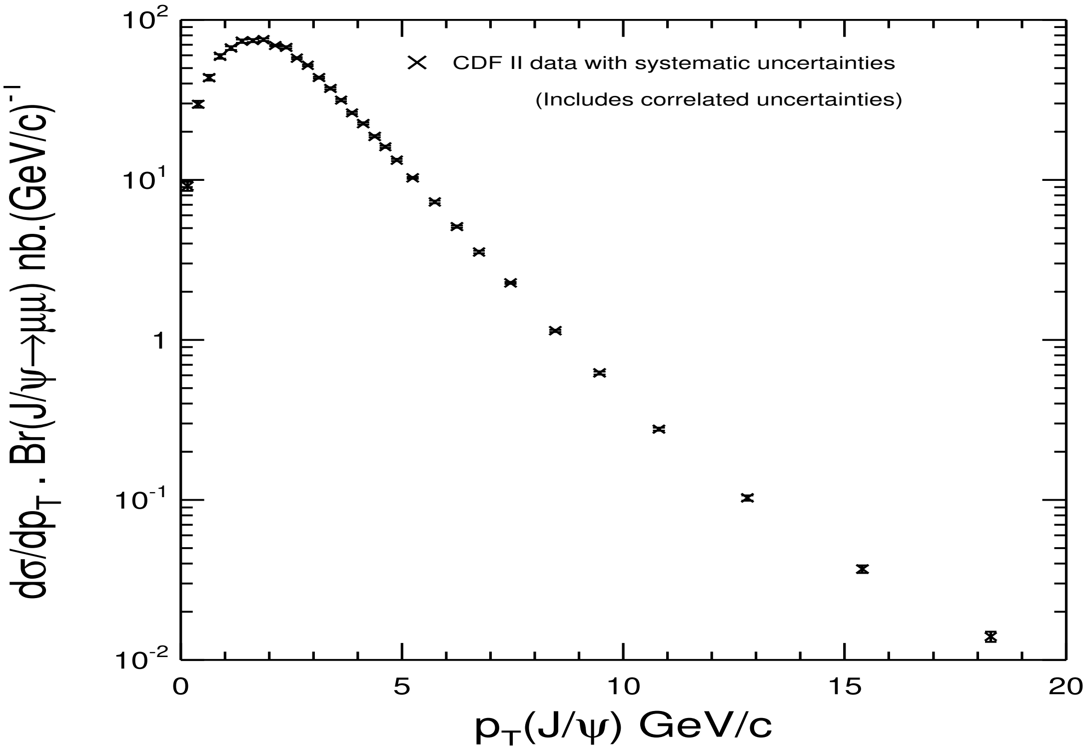

Figure 16: Inclusive J/ψ cross-section as a function of J/ψ p_T. The differential cross section with systematic and statistical uncertainties added is plotted.

$|\eta| < 0.6$. Therefore this measurement integrated over $|\eta| < 0.6$ is:

$$\sigma(p\overline{p} \to J/\psi X, p_T(J/\psi) > 5.0 GeV/c, \mid \eta(J/\psi) \mid < 0.6)_{RunII} = 16.3 \pm 0.1(stat)^{+1.4}_{-1.3}(syst) \text{ nb}$$

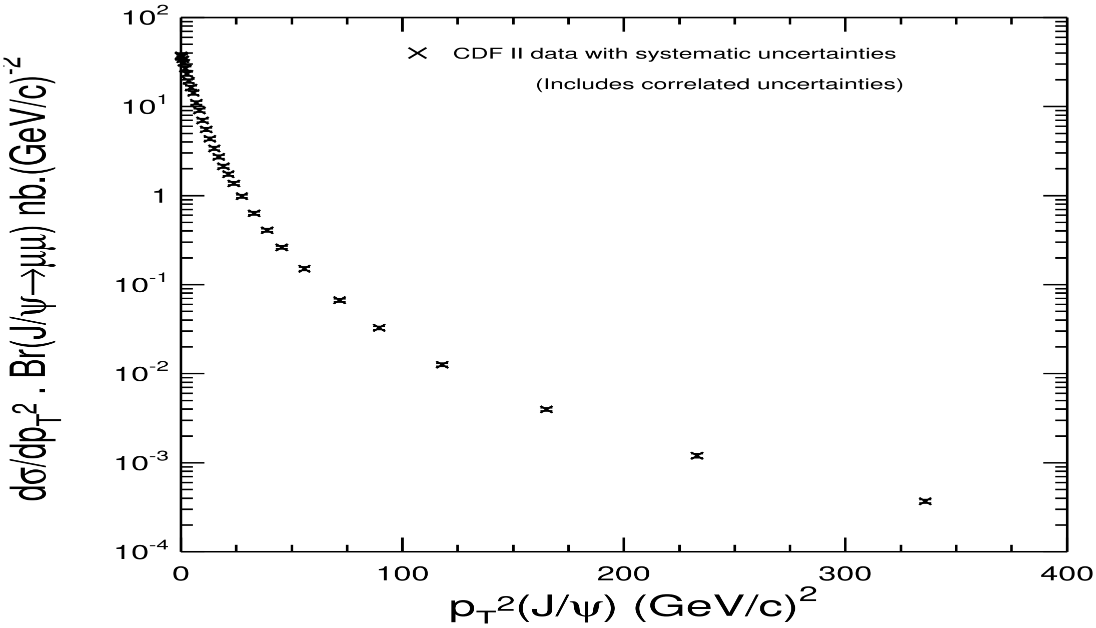

Figure 17: Inclusive J/ψ cross-section as a function of J/ψ p_T^2. The differential cross-section with statistical and systematic uncertainties added is plotted.

The equivalent Run I measurement was

$$\sigma(p\overline{p} \rightarrow J/\psi X, p_T(J/\psi) > 5.0GeV/c, \mid \eta(J/\psi) \mid < 0.6)_{RunI} = 17.4 \pm 0.1(stat)^{+2.6}_{-2.8}(syst) \text{ nb}$$

Although the Run II cross-section is measured at a higher center-of-mass, and its expected that the production cross-sections increase by $10 \pm 5\%$, the Run I and Run II measurements are still consistent within measurement errors.

7 Summary

A preliminary measurement of the inclusive J/ψ cross section in CDF Run-II was made. The total integrated cross section for inclusive J/ψ production in $p\bar{p}$ interactions at C.O.M. energy, $\sqrt{s} = 1960$ GeV/c^2, is measured to be:

$$\sigma(p\overline{p} \rightarrow J/\psi X, \mid y(J/\psi) \mid < 0.6) = 240 \pm 1(stat) \pm 21(syst) \text{ nb}$$

.

The integrated crossection for $p_T(J/\psi) > 5.0$ GeV/c and $|\eta| < 0.6$ in Run II was measured to be:

$$\sigma(p\overline{p} \rightarrow J/\psi X, p_T(J/\psi) > 5.0GeV/c, \mid y(J/\psi) \mid < 0.6)_{RunII} = 16.3 \pm 0.1(stat)^{+1.4}_{-1.3}(syst) \text{ nb}$$

which is in good agreement with the Run I measurement of:

$$\sigma(p\overline{p} \to J/\psi X, p_T(J/\psi) > 5.0 GeV/c, \mid \eta(J/\psi) \mid < 0.6) = 17.4 \pm 0.1(stat)^{+2.6}_{-2.8}(syst) \text{ nb}$$

The differential cross-section results are summarized in Table 14.

P_t range GeV/c	Yield	Acceptance	L1 Trigger eff	Track-stub matching eff.
$0.0 - 0.25$	365 ± 25	$0.0153^{+0.0007}_{-0.0007}$	$0.857^{+0.011}_{-0.013}$	0.9963 ± 0.0009
$0.25 - 0.5$	605 ± 30	$0.0069^{+0.0004}_{-0.0004}$	$0.860^{+0.011}_{-0.013}$	0.9963 ± 0.0009
$0.5 - 0.75$	962 ± 38	$0.0070^{+0.0004}_{-0.0004}$	$0.865^{+0.011}_{-0.013}$	0.9962 ± 0.0009
$0.75 - 1.0$	1592 ± 49	$0.0087^{+0.0005}_{-0.0004}$	$0.871^{+0.012}_{-0.014}$	0.9961 ± 0.0009
$1.0 - 1.25$	2500 ± 62	$0.0116^{+0.0006}_{-0.0006}$	$0.877^{+0.012}_{-0.014}$	0.9960 ± 0.0009
$1.25 - 1.5$	3549 ± 74	$0.0151^{+0.0008}_{-0.0007}$	$0.885^{+0.013}_{-0.014}$	0.9957 ± 0.0009
$1.5 - 1.75$	4517 ± 84	$0.0190^{+0.0009}_{-0.0009}$	$0.892^{+0.013}_{-0.014}$	0.9955 ± 0.0009
$1.75 - 2.0$	5442 ± 93	$0.0232^{+0.0011}_{-0.0010}$	$0.899^{+0.014}_{-0.015}$	0.9953 ± 0.0009
$2.0 - 2.25$	16059 ± 167	$0.0271^{+0.0013}_{-0.0012}$	$0.905^{+0.014}_{-0.015}$	0.9960 ± 0.0009
$2.25 - 2.5$	18534 ± 252	$0.0317^{+0.0015}_{-0.0013}$	$0.911^{+0.014}_{-0.015}$	0.9946 ± 0.0009
$2.5 - 2.75$	18437 ± 253	$0.0367^{+0.0017}_{-0.0016}$	$0.916^{+0.014}_{-0.015}$	0.9943 ± 0.0009
$2.75 - 3.0$	18858 ± 259	$0.0415^{+0.0019}_{-0.0018}$	$0.920^{+0.015}_{-0.015}$	0.9939 ± 0.0009
$3.0 - 3.25$	18101 ± 253	$0.0467^{+0.0021}_{-0.0019}$	$0.924^{+0.015}_{-0.015}$	0.9935 ± 0.0009
$3.25 - 3.5$	17597 ± 250	$0.0532^{+0.0024}_{-0.0022}$	$0.927^{+0.015}_{-0.015}$	0.9931 ± 0.0009
$3.5 - 3.75$	16400 ± 241	$0.0576^{+0.0025}_{-0.0023}$	$0.930^{+0.015}_{-0.015}$	0.9927 ± 0.0009
$3.75 - 4.0$	14863 ± 226	$0.0628^{+0.0029}_{-0.0027}$	$0.932^{+0.015}_{-0.015}$	0.9923 ± 0.0009
$4.0 - 4.25$	14056 ± 218	$0.0694^{+0.0031}_{-0.0030}$	$0.934^{+0.015}_{-0.015}$	0.9918 ± 0.0010
$4.25 - 4.5$	12719 ± 212	$0.0768^{+0.0034}_{-0.0032}$	$0.936^{+0.015}_{-0.015}$	0.9913 ± 0.0010
$4.5 - 4.75$	12136 ± 201	$0.0840^{+0.0037}_{-0.0035}$	$0.937^{+0.014}_{-0.014}$	0.9909 ± 0.0010
$4.75 - 5.0$	10772 ± 188	$0.0904^{+0.0039}_{-0.0037}$	$0.939^{+0.014}_{-0.014}$	0.9904 ± 0.0010
$5.0 - 5.5$	18478 ± 241	$0.1006^{+0.0042}_{-0.0039}$	$0.940^{+0.014}_{-0.014}$	0.9897 ± 0.0010
$5.5 - 6.0$	14616 ± 210	$0.1130^{+0.0046}_{-0.0044}$	$0.942^{+0.014}_{-0.014}$	0.9887 ± 0.0011
$6.0 - 6.5$	11388 ± 180	$0.1257^{+0.0051}_{-0.0047}$	$0.946^{+0.014}_{-0.014}$	0.9876 ± 0.0011
$6.5 - 7.0$	8687 ± 154	$0.1397^{+0.0055}_{-0.0054}$	$0.945^{+0.014}_{-0.014}$	0.9865 ± 0.0012
$7.0 - 8.0$	12409 ± 139	$0.1561^{+0.0068}_{-0.0066}$	$0.946^{+0.014}_{-0.014}$	0.9850 ± 0.0012
$8.0 - 9.0$	6939 ± 107	$0.1723^{+0.0075}_{-0.0072}$	$0.947^{+0.014}_{-0.014}$	0.9827 ± 0.0013
$9.0 - 10.0$	3973 ± 78	$0.1807^{+0.0079}_{-0.0077}$	$0.948^{+0.014}_{-0.014}$	0.9804 ± 0.0014
$10.0 - 12.0$	3806 ± 74	$0.1938^{+0.0074}_{-0.0072}$	$0.949^{+0.014}_{-0.014}$	0.9772 ± 0.0016
$12.0 - 14.0$	1566 ± 49	$0.2163^{+0.0081}_{-0.0080}$	$0.960^{+0.014}_{-0.014}$	0.9726 ± 0.0017
$14.0 - 17.0$	935 ± 40	$0.2380^{+0.0081}_{-0.011}$	$0.951^{+0.014}_{-0.014}$	0.9671 ± 0.0018
$17 - 20.0$	350 ± 25	$0.247^{+0.012}_{-0.010}$	$0.951^{+0.013}_{-0.014}$	0.9600 ± 0.0020

Table 14: Summary of J/ψ cross-section results. The values of the yield and statistical uncertainty from the fit is listed in the 2nd column. The acceptance values and the combined systematic and statistical uncertainties on the acceptance are listed in the 3rd column. In the fourth and fifth columns the trigger and track-stub matching efficiencies obtained from the mean of the distribution in each transverse J/ψ momentum bin and the corresponding systematic uncertainties are listed.

8 Acknowledgements

We would like to thank the following people for their invaluable insights and help in completing this study:

The muon and COT validation groups, Ken Bloom, Peter Wittich, Larry Nodulman, Aseet Mukherjee, Vaia Papadimitrou.

References

[1] CDF Collaboration. F.Abe *et al.*, Phys.Rev.Lett. **79**, 572 (1997).

[2] J. Binnewies, Bernd A. Kniehl and G. Kramer, Phys. Rev. D58 034016 (1998).

[3] Matteo Cacciari and Paolo Nason, Phys. Rev. Lett. 89 122003 (2002).

[4] P.Cho and A.K.Leibovich, Phys.Red.**D53**,150(1996).

[5] Adam K. Leibovich, Nucl. Phys. Proc. Suppl. **93** 182 (2001).

[6] R. Baier and R.Ruckl, Z.Phys. **C19**. 251 (1983)

[7] Eric Braaten, Sean Fleming, Adam Leibovich, Phys. Rev. **D 63** 094006 (2001).

[8] Y.Gotra *et al.*, CDF/PHYS/TRIGGER/PUBLIC/6162, "Run-II Muon Trigger Efficiency Measurement".

[9] M. Bishai *et al.* ,CDF/DOC/BOTTOM/CDFR/6144

[10] Information on the good run DB bits can be found at http://nucl02.fnal.gov/~snihur/val/offval.html

[11] The criteria for COT good run list is:

Good COT operation: condition (full coverage with 100% HV)

Good Run bit = 1 & Analysis Run bit = 1 (tagged by shift crew);

Integrated luminosity > 10 $nb - 1$;

Number of bad channels < 1%.

More detail and development can be found in

"//www-cdf.fnal.gov/internal/people/links/Young-KeeKim/COT_Validation.html"

[12] CMU hits distribution, coverages and track-stub matching were carefully checked and detail is in:

http://lotus.phys.nwu.edu/ schmittm/cdfmuon/

[13] Details of the selection of the J/ψ good run list can be found in the summary and meeting minutes of the bottom validation groups web page at:

http://www-cdf.fnal.gov/internal/physics/bottom/validation/

[14] John R. Taylor, " An Introduction to Error Analysis ". University Science Books, 1982

[15] Instructions on the official luminosity web page:
http://www-cdf.fnal.gov/internal/people/links/JacoboKonigsberg/lum_official_page.htm

The FIRST STEP in finding the integrated luminosity for a given dataset is to generate a LOG FILE with a list of runs and run-sections that correspond to the ORIGINAL POOL from which this dataset was created. This is done through the AC++ Data Handling Input module as follows:

```
AC++> Mod Talk DHInput
      luminosityLog set your_log_file_name.rsl
```

The SECOND STEP consists in running a standalone program that input this log file and that sums all the corresponding entries in the Data File Catalogue:

```
fcdfsgi2> lumsum.pl offline your_log_file_name.rsl
```

This program has been created by the Data Handling group (Eric Wicklund) and runs on FCDFSGI2 after the standard setups:

```
fcdsgi2> source ~cdfsoft/cdf2.cshrc
fcdfsgi2> setup cdfsoft2 4.2.0 (or any other version)
```

[16] J. Konigsberg *et al.*, /CDF/ANAL/CDF/CDFR/6052

[17] S. Klimenko *et al.*, /CDF/DOC/CDF/CDFR/6314

[18] T. LeCompte, /CDF/ANAL/MUON/CDFR/6114

[19] K. Anikeev *et al.*,/CDF/DOC/BOTTOM/CDFR/6022

[20] Particle Data Group. The European Physical Journal **3** 1998 (582)

[21] C. Chen *et al.*,/CDF/DOC/BOTTOM/CDFR/CDFNOTE 6394.

[22] Ken Bloom *al.*, /CDF/ANAL/MUON/CDFR/6347

[23] The CDF II Detector Technical Design Report, November 1996.

[24] CotSim is a hit level COT simulation and track fitter written by R. Culbertson and adapted by Ashutosh Kotwal. It includes multiple scattering and ionization energy loss in the COT and upstream material. The ionization eloss is calculated using the Bethe-Bloch equation including the density effect. The SVXII material is modeled using SiliMap v4.9.0 a 3-D material map extracted from the GEANT description of the detector. In addition dE/dX corrections obtained from Cosmic Ray studies, and corrections to the B-Field are included.

[25] http://www-cdf.fnal.gov/cdfsim/cdfsim_generators.html#generators

[26] http://cdfcodebrowser.fnal.gov/CdfCode/source/Extrapolator/Extrapolator/MExtrapolator.h

[27] http://www.hep.anl.gov/lecompte/Public/cdf/muonplots.html

[28] CDF Collaboration. F.Abe *et al.*, Phys.Rev.Lett. **85**, 2886 (2000).

[29] R. Cropp *et al.*,/CDF/ANAL/BOTTOM/CDFR/5029

[30] T. LeCompte, /CDF/MEMO/BOTTOM/CDFR/6090

[31] Private communication with A. Mukherjee and J.C. Yun.

[32] J. Gonzalez *al.*, CDF/ANAL/BOTTOM/CDFR/3010

[33] P Azzi *al.* CDF/DOC/TRACKING/CDFR/5562

[34] Private communication with Peter Wittich

[35] K. Bloom*et al.*, CDFNOTE 6017.

List of Tables

List of Figures